PERGAMON

International Journal of Plasticity 16 (2000) 893–949

INTERNATIONAL JOURNAL OF Plasticity

www.elsevier.com/locate/ijplas

Structural changes in elastoplastic material: a unified finite-element approach to phase transformation, twinning and fracture

Alexander V. Idesman [a,*], Valery I. Levitas [b], Erwin Stein [a]

[a] *Institute of Structural and Computational Mechanics, University of Hannover, Appelstraße 9A, D-30167 Hannover, Germany*

[b] *Texas Tech University, Department of Mechanical Engineering, Lubbock, TX 79409-1021, USA*

Received in final revised form 23 September 1999

Abstract

A unified finite-element approach to phase transformation (PT), twinning and fracture in elastoplastic materials both at small and finite strains is developed. The applicability of the approach is illustrated by numerical solutions of a number of two-dimensional elastoplastic boundary-value problems, in particular, layer by layer PT progress in a cylindrical specimen, adiabatic strain-induced PT at shear-band intersection and in a spherical particle imbedded in a cylindrical specimen, appearance and growth of a temperature-induced martensitic plate in austenitic matrix, furthermore the appearance of a single twin in an elastoplastic matrix under applied shear stress or displacement, fracture in a sample with an edge notch and an interaction between PT and fracture in the same sample. Both time independent and time dependent kinetics are considered. For time independent kinetics, in order to overcome nonuniqueness of solution of boundary-value problems due to competition between phase transition and plasticity and/or fracture, the global phase transition and fracture criteria based on stability analysis are applied. The solutions obtained give insight into various effects, in particular the very complex and nontrivial strain field variations and their influence on the driving force for structural changes, the peculiarity of interaction between phase transformation, twinning, fracture and plasticity, effect of strain hardening and adiabatic heating, formation of a discrete microstructure at phase transition and fracture (in particular, void nucleation ahead of the crack tip rather than continuous crack propagation). Some of the numerical results for the driving force are approximated analytically and applied to the analytical determination of the geometry of phase transformation and fracture zone based on the corresponding extremum principle.

Keywords: A. Phase transformation; A. Fracture; B. Elastic–plastic material; B. Finite strain; C. Finite elements

* Corresponding author. Tel.: +49-511-762-5496; fax: +49-511-762-5498.
E-mail address: idesman@leibniz.ibnm.uni-hannover.de (A.V. Idesman).

0749-6419/00/$ - see front matter
PII: S0749-6419(99)00082-0

1. Introduction

Recently a new continuum thermomechanical and kinetic approach has been developed for the description of a wide class of structural changes (SC) in inelastic materials, which includes PT, twinning, fracture, strain-induced chemical reactions (see Levitas 1998a,b,c, 2000a,b; Levitas et al., 1998b). To illustrate the approach, which is based on a consideration of SC in some volume without introducing the volume fraction (i.e. it includes a detailed description of SC with sharp interfaces between phases) some simple analytical solutions are obtained and analyzed, in particular for PT in an ellipsoidal inclusion under prescribed shear stress (Levitas, 1998c, 2000a,b), PT in a spherical inclusion at a given pressure (Levitas, 2000a,b), chemical reactions in a shear band (Levitas et al., 1998b; Levitas, 1998c, 2000a,b), spherical void nucleation and crack propagation in a similar framework as the Dugdale model for a plane stress state (Levitas 1998b, 2000a,b).

To consider more complex and real problems, appropriate numerical methods have to be developed. The aim of this paper is to develop a unified finite element approach to phase transformation, twinning and fracture in elastoplastic materials both at small and finite strains. Previously numerical approaches to a description of PT in some volume of elastoplastic material with small strains and coherent interfaces were given in the papers by Leblond (1989), Leblond et al. (1989), Ganghoffer et al. (1991), Marketz and Fischer (1994a,b), Reisner et al. (1998), Levitas et al. (1998a). The analysis of some of them can be found in the papers by Levitas et al. (1998a). A simple numerical approach to the description of incoherent interfaces and interfaces with decohesion was suggested in the papers by Idesman et al. (1997a), Levitas et al. (1998a). A numerical method for the thermodynamic description of PT and twinning at finite strains were recently published in a paper by Idesman et al. (1999b). Kinetic aspects of PT, consideration of fracture as a deformation process in a finite volume as well as the interaction between fracture and PT in elastoplastic materials are presented here for the first time. The applicability of this approach is illustrated by solutions of a number of two-dimensional boundary-value problems.

In Section 2 a problem formulation for martensitic PT in elastoplastic isotropic materials both at small and finite strains is presented. The considered problem formulation at finite strains includes finite plastic and transformation strains and small elastic deformations. The deformation model is based on the multiplicative decomposition of the total deformation gradient into elastic, transformation and plastic parts. In contrast to our first papers on PT at finite strains (Idesman et al., 1997b, 1999a), where a symmetric plastic deformation gradient is assumed, a non–symmetric plastic deformation gradient is used. An additional condition of zero modified plastic spin is derived for isotropic materials, instead of assuming the symmetry of the plastic deformation gradient. Such an approach is also very convenient from a computational point of view (Idesman et al., 1999b). A complete set of kinematic and constitutive equations for plasticity is presented in Sections 2.1 and 2.2. Conditions for coherent and incoherent interfaces as well as interfaces with decohesion are described in Section 2.3. Thermodynamic criteria and a kinetic equation for SC are presented in Section 2.4 for time independent and thermally activated kinetics. Particular cases of

driving forces for PT, twinning and fracture are considered. Extremum principles for the determination of location and volume of the transformed region are presented in Section 2.5. For time dependent kinetics the extremum principle corresponds to the minimum of transformation time, or in a particular case to the minimum of transforming mass combined with the thermodynamic SC criterion. In addition, for time independent kinetics a global criterion of SC based on stability analysis is analyzed.

The finite element algorithm for determination of the stress and strain variations during SC at the given SC region, briefly discussed in Section 3, is realized at finite strains in a step-by-step form with a variable actual configuration. The use of the current configuration and the true Cauchy stresses along with assumptions of small elastic strains and the condition of zero modified plastic spin allows us to apply the radial return algorithm and to derive quite a simple formula for the consistent elastoplastic moduli.

In Section 4.1 layer by layer PT progress in a cylindrical specimen is studied. It is demonstrated that depending on the applied stress and the elastoplastic properties either continuous interface propagation or formation of a discrete microstructure follows from the extremum principle used. In Section 4.2 one aspect of nucleation at shear-band intersection, namely allowing for adiabatic heating during the PT, is studied. The result is obtained that the effective temperature which appears in the PT criterion and the kinetic equation differs by 67 K from the transformation start temperature. This difference is quite important and is mostly due to transformation heat. Application of the global PT criterion based on stability analysis is illustrated in Section 4.3 using the solution of the problem of strain-induced PT in a spherical particle imbedded in a cylindrical specimen.

The problems of the appearance of a temperature-induced martensitic plate in an austenitic matrix are solved and analyzed in Section 4.4. Explicit expressions for the width and length of the plate are obtained in terms of material properties. The following typical cases in the determination of the geometric parameters of the plate are found: solely from the principle of the minimum of transformation time and the kinetic equation without any constraints; from the principle of the minimum of transformation mass and the thermodynamic criterion of SC; furthermore as an interatomic distance and from the thermodynamic criterion.

The growth of the martensitic plate in an austenitic matrix mentioned above is studied in Section 4.5. Very complex and heterogeneous stress-strain fields in austenite and martensite and their nonmonotonous time variation are obtained. Plastic shear strain at some points can reach 60% and, after some elastic stage, changes its sign and vary for about 40% in the opposite direction. The profile of the moving interface (the short side of a plate) varies in a nontrivial way as well: after the expected profile corresponding to transformation shear, it follows the wave-like profile with the resulting shear strain near the corners directed in the opposite direction to the transformation shear, and finally ends up in a practically undeformed vertical line (as before transformation). These results demonstrate the necessity of finite strain treatment. After the appearance of the martensitic plate, transformation work decreases by a factor of two during the lengthening of the plate by 10%. This can lead to growth arrest of martensitic plates.

The appearance of a single twin in an elastoplastic material under applied shear stress is considered in Section 4.6.

Various scenarios of fracture in a sample with an edge notch are investigated in Section 5. At a relatively small surface energy, a void nucleation occurs rather than crack (notch) growth. After a void nucleation fracture propagates in the direction from void to notch. Using an analytical approximation of some numerical results obtained, the width and length of the fracture zone are obtained analytically. Typical cases for the determination of two characteristic sizes of fracture region are similar to those for a temperature-induced martensitic plate.

An interaction between PT and fracture in the same sample is described in Section 6. In particular, an application of the global PT and fracture criteria are used to analyze the competition between fracture and PT.

The analysis of some known solutions related to the interaction between PT and plasticity, including our results, is presented in the paper as well.

Direct tensor notations are used throughout this paper. Vectors and tensors are denoted in boldface type; $\mathbf{A}\cdot\mathbf{B}$ and $\mathbf{A}:\mathbf{B}$ are the contraction of tensors over one and two indices; $\mathbf{I}$ is the unit second-rank tensor; dev$\mathbf{A}$ is the deviatoric part of $\mathbf{A}$; $|\mathbf{A}| := (\mathbf{A}:\mathbf{A}^{t})^{1/2}$ is the amplitude of tensor $\mathbf{A}$. A superscripts t and -1 denote transposed and inverse operations; subscripts s and a designate symmetrical and antisymmetrical tensor parts; $:=$ means equals per definition; a point above indicates the material time derivative, the indices 1 and 2 denote the values before and after SC.

2. Problem formulation at finite strains

Consider a volume V of the multiphase material with a boundary S and prescribed boundary data. Assume that some volume V_n with a fixed boundary Σ_n relative to the material points undergoes some SC which include martensitic PT, twinning and fracture as particular cases in this paper. Martensitic PT is considered as a special type of deformation of a crystal lattice from the parent phase (austenite) into a crystal lattice of product phase (martensite) without diffusion, see Fig. 1a, which is accompanied by a jump in all the thermomechanical properties. This deformation is called the transformation strain. The transformation deformation gradient cannot be arbitrary (as the elastic or plastic strain). For each PT the right stretch transformation tensor is a fixed tensor to within symmetry operations. All intermediate values of the transformation right stretch tensor are unstable and cannot exist in an equilibrium. Twinning will be described as a particular case of martensitic PT without any change in material properties during twin appearance. The transformation strain in twinning has only shear components, Fig. 1b.

Formally we use the following general definition of SC (Levitas, 2000a,b):

The SC is considered as a process of variation of the transformation deformation gradient and some or all thermomechanical properties in a transforming volume from the initial to final value. This process cannot be stopped at an intermediate state in any transforming point.

We consider here such an SC as displacive PT, twinning and fracture. For PT we will neglect the change in elastic properties, i.e. PT is a thermomechanical process of

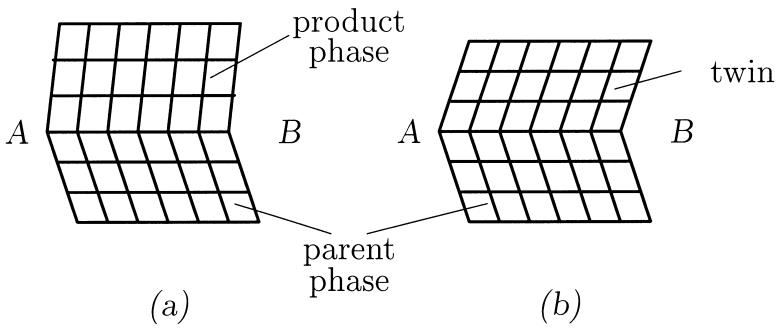

Fig. 1. Deformation due to transformation for phase transformation (a) and twinning (b).

growth of a transformation deformation gradient (or transformation strain in the case of small strains) in some transforming region V_n from unit tensor $\mathbf{I}$ (from zero for the transformation strain in case of small strains) to a final value which is accompanied by a change in thermal properties. Twinning will be treated as a particular case of PT without any change in thermal properties and when the transformation strain is simple shear. Fracture is another particular case without transformation strain, i.e. fracture will be considered as a thermomechanical process of decrease in Young's modulus E and the yield stress σ_y from the initial value to zero.

2.1. Kinematics

Let the motion of the uniformly deformed infinitesimal volume in a process of SC be described by the function $\mathbf{r} = \mathbf{r}(\mathbf{r}_\tau, t)$, where $\mathbf{r}$ and $\mathbf{r}_\tau$ are the positions of points in the actual V_n and the reference V_n^τ (at $t = 0$) configurations, $\mathbf{u} = \mathbf{r} - \mathbf{r}_\tau$ is the displacement of a material point, t is the current time. Thermal strains are neglected because they are small with respect to transformation strains. We present only the final set of equations (given in Box 1) in a form convenient for numerical algorithms (for the derivation see Idesman et al., 1999b).

For small strains we use a linear decomposition of the total strain $\boldsymbol{\varepsilon}$ into elastic $\boldsymbol{\varepsilon}_e$, plastic $\boldsymbol{\varepsilon}_p$ and transformation $\boldsymbol{\varepsilon}_t$ parts, see Box 1. We introduce the dimensionless order parameter ξ $(0 \leqslant \xi \leqslant 1)$ in Eq. (9) for PT and twinning and in Eq. (10) for fracture. SC starts at $\xi = 0$ and finishes at $\xi = 1$.

For finite strains we assume a multiplicative decomposition of the total deformation gradient $\mathbf{F} = \frac{\partial \mathbf{r}}{\partial \mathbf{r}_\tau}$ into elastic $\mathbf{F}_e$, transformational $\mathbf{F}_t$ and plastic $\mathbf{F}_p$ parts, see Eq. (12), where $\mathbf{F} = \mathbf{V}_e \cdot \mathbf{R}_e$; $\mathbf{V}_e$ is the elastic left stretch (symmetric) tensor, $\mathbf{R}_e$ is the elastic rotation tensor. The order parameter ξ is defined for PT and twinning by Eq. (14) and varies from 0 to 1 when the transformation deformation gradient grows from $\mathbf{I}$ to the final maximum value $\mathbf{F}_{t2}$ determined by crystallography. For twinning, the transformation deformation gradient represents a simple shear γ_t of the crystal lattice accomplished in shear direction $\mathbf{m}$ across the plane with normal $\mathbf{n}$, i.e. $\mathbf{F}_t = \mathbf{I} + \gamma_t \mathbf{mn}$. For a small strain $\boldsymbol{\varepsilon}_t = \gamma_t(\mathbf{mn})_s$. In both cases $\xi = \frac{\gamma_t}{\gamma_{t2}}$, where γ_{t2} is the shear of the crystal lattice at the end of PT.

For fracture the parameter ξ is defined by Eq. (15) which is the same as at small strains. Here E and E_1 are the Young's moduli during and before PT respectively. We assume that during a fracture process the yield stress σ_y is changed proportional to E.

Using Eq. (12) the velocity gradient $\mathbf{l}$ and deformation rate $\mathbf{d}$ are decomposed as follows

$$\begin{aligned}\mathbf{l} &:= \frac{\partial \boldsymbol{\upsilon}}{\partial \mathbf{r}} = \dot{\mathbf{F}}\cdot\mathbf{F}^{-1} = \dot{\mathbf{F}}_e\cdot\mathbf{F}_e^{-1} + \mathbf{F}_e\cdot\dot{\mathbf{F}}_t\cdot\mathbf{F}_t^{-1}\cdot\mathbf{F}_e^{-1} + \mathbf{F}_e\cdot\mathbf{F}_t\cdot\dot{\mathbf{F}}_p\cdot\mathbf{F}_p^{-1}\cdot\mathbf{F}_t^{-1}\cdot\mathbf{F}_e^{-1}\\ &= \dot{\mathbf{F}}_e\cdot\mathbf{F}_e^{-1} + \mathbf{l}_t + \mathbf{l}_p,\end{aligned} \tag{1}$$

$$\mathbf{d} := (\mathbf{l})_s = (\dot{\mathbf{F}}_e\cdot\mathbf{F}_e^{-1})_s + \mathbf{d}_t + \mathbf{d}_p, \tag{2}$$

where $\boldsymbol{\upsilon} = \dot{\mathbf{r}}$ is the velocity vector, $\mathbf{l}_t$ and $\mathbf{l}_p$ are the transformational and the plastic parts of the velocity gradients, $\mathbf{d}_t = (\mathbf{l}_t)_s$ and $\mathbf{d}_p = (\mathbf{l}_p)_s$ are the transformational and the plastic parts of the deformation rate (see Box 1).

To define uniquely the elastic and plastic parts of the total deformation gradient we use the condition that the modified plastic spin is zero, i.e.

$$\mathbf{w}_p := (\mathbf{l}_p)_a = (\mathbf{F}_e\cdot\mathbf{F}_t\cdot\dot{\mathbf{F}}_p\cdot\mathbf{F}_p^{-1}\cdot\mathbf{F}_t^{-1}\cdot\mathbf{F}_e^{-1})_a = 0 \quad \text{and} \quad \mathbf{d}_p = \mathbf{l}_p. \tag{3}$$

This constitutive result can be derived for isotropic materials by some extension and application of a method developed by Levitas (1998d) for the case with PT. Here we use another method of derivation of Eq. (3) similar to that developed by Dafalias (1984) for materials without PT. Assume that the modified plastic spin $\mathbf{w}_p$ is a function of the plastic part of the deformation rate $\mathbf{d}_p$ and the Cauchy stress tensor $\mathbf{T}$, i.e.

$$\mathbf{w}_p := \left(\mathbf{F}_e\cdot\mathbf{F}_t\cdot\dot{\mathbf{F}}_p\cdot\mathbf{F}_p^{-1}\cdot\mathbf{F}_t^{-1}\cdot\mathbf{F}_e^{-1}\right)_a = f(\mathbf{d}_p, \mathbf{T}). \tag{4}$$

Using the representation theorem (Dafalias, 1984) the expression for the modified plastic spin $\mathbf{w}_p$ can be written as

$$\begin{aligned}\mathbf{w}_p = f(\mathbf{d}_p, \mathbf{T}) &= \eta_1(\mathbf{d}_p\cdot\mathbf{T})_a + \eta_2(\mathbf{d}_p^2\cdot\mathbf{T})_a + +\eta_3\left(\mathbf{d}_p\cdot\mathbf{T}^2\right)_a + \eta_4\left(\mathbf{d}_p\cdot\mathbf{T}\cdot\mathbf{d}_p^2\right)_a\\ &+ \eta_5\left(\mathbf{T}\cdot\mathbf{d}_p\cdot\mathbf{T}^2\right)_a,\end{aligned} \tag{5}$$

where η_i are the functions of invariants of tensors $\mathbf{d}_p$ and $\mathbf{T}$. For isotropic materials tensors $\mathbf{d}_p$ and T are coaxial [see constitutive Eq. (23)] and all the terms in the right part of Eq. (5) are zero and $\mathbf{w}_p = 0$.

A similar condition for $\mathbf{w}_p$ is accepted in many papers on large strains without PT, see for example Weber and Anand (1990); Cuitino and Ortiz (1992). It allows us to determine the rate of plastic deformation gradient $\dot{\mathbf{F}}_p$ through the rate of plastic deformation $\mathbf{d}_p$ (see below).

In our first papers on PT simulations at finite strains (Idesman et al., 1997b, 1999a) we used in Eqs. (12) and (18) the symmetric plastic deformation gradient $\mathbf{U}_p$ with 6 components instead of $\mathbf{F}_p$ with 9 components as here. Therefore, we did not need additional equations like Eq. (3) (3 equations in a component form). But the final equations in the papers by Idesman et al. (1997b,1999a) are more complicated for calculations, as we have to use objective derivatives in a numerical scheme.

For the description of elastic strain we use the elastic strain tensor $\mathbf{B}_e$ defined by Eq. (13). We assume that the elastic strains are small, i.e. $\mathbf{V}_e = \mathbf{I} + \boldsymbol{\varepsilon}_e$, $\boldsymbol{\varepsilon}_e \ll \mathbf{I}$, then $\mathbf{V}_e^{-1} \approx \mathbf{I} - \boldsymbol{\varepsilon}_e$ and $\mathbf{B}_e \approx \boldsymbol{\varepsilon}_e$.

In the approach presented the transformation deformation gradient $\mathbf{F}_t$ should be prescribed as input data. For the solution of the PT problem we vary it according to Eq. (16). The final value of the transformation deformation gradient $\mathbf{F}_{t2}$ is determined in this paper according to the crystallographic theory of PT [see Wechsler, Lieberman & Read, 1953; Nishiyama, 1978). This means that the transformation strain corresponds to a deformation with an invariant (nondeformable and nonrotating) plane, which is called a habit plane.

For a material point without PT we must prescribe in the equations presented above that $\mathbf{F}_t = \mathbf{I}$ for deformation before PT or $\mathbf{F}_t = \mathbf{F}_{t2} = \text{const}$ for deformation after PT.

2.2. Constitutive equations

We use the thermodynamically consistent system of the constitutive equations for isotropic elastoplastic materials with PT and isotropic hardening which have the same form at small and finite strains and presented in Box 1, Eqs. (21)–(24). Detailed derivation of these equations can be found in the paper by Idesman et al. (1999b). Here q is the accumulated plastic strain; $\sigma_i = (3/2\mathbf{s} : \mathbf{s})^{1/2}$ is the stress intensity; $\mathbf{s} = dev\mathbf{T}$ is the deviatoric part of the Cauchy stress tensor $\mathbf{T}$; $\sigma_y(q, \xi)$ is the yield stress, a function to be found experimentally; $\mathbf{E}$ is the elastic modulus tensor; K and G are the bulk and shear elastic moduli; $I_1(\boldsymbol{\varepsilon}_e) = \mathbf{I} : \boldsymbol{\varepsilon}_e$ is the first invariant of $\boldsymbol{\varepsilon}_e$.

2.3. Incoherent interface and interface with decohesion

Under some circumstances displacement discontinuities across the interface can occur which significantly affect PT conditions. We have developed a simple way of admitting incoherence (sliding) and decohesion by treating them as a contact problem (Levitas, 1997,1998a; Idesman et al., 1997a; Levitas et al., 1998a). Three types of interfaces between new and old phases are considered: coherent (with continuous displacements across the interface), incoherent (with discontinuous tangential displacements across the interface) and the interface with decohesion (with crack at the interface). We assume that PT and incoherence (decohesion) criteria are thermodynamically mutually independent and that these processes are coupled through the stress fields only. If during the growth of $\mathbf{F}_t$ (or $\boldsymbol{\varepsilon}_t$ in case of small strains) and variation of material thermomechanical properties in a nucleus a chosen decohesion

criterion is met at some point of the interface, the crack appears or grows. If with the variation of $\mathbf{F}_t$ the incoherence criterion is satisfied, we admit sliding in this point until a value where the criterion is violated. After completing the PT we check with the PT criterion whether PT is thermodynamically admissible. Consequently, the growing transformation deformation gradient $\mathbf{F}_t$ generates the stresses which are necessary for the appearance of decohesion or incoherence, and decohesion and incoherence change the stress variation in the transforming particle. As the simplest decohesion (incoherence) criterion we assume that, if the normal to interface tensile (or shear) stress reaches some critical value, then the fracture (or sliding) in this point occurs. These conditions are given in Box 1, where $\sigma_n\mathbf{n}$ and $\boldsymbol{\tau}_c$ are normal and tangential stresses at the interface; $\mathbf{n}$ is the unit normal to the interface, σ_c and τ_s are critical values of normal and shear stresses; $\dot{u}_n\mathbf{n}, \dot{\mathbf{u}}_\tau$ are the normal and tangential velocity at the interface; λ_1 is the positive multiplier, the upper indices 1 and 2 identify those belonging to the parent and the product phases.

There is an alternative, a much more detailed and consequently complex way to treat displacement discontinuity. One can consider nucleation of discrete dislocations and cracks at the interface as additional structural change and apply the same theory of SC.

2.4. Thermodynamics and kinetics of SC

The key points of our approach are as follows (Levitas, 1998b,c, 2000a,b). Using the second law of thermodynamics, the dissipation rate due to SC only, $\mathcal{D}$, is separated from other dissipative contributions (e.g. due to plastic deformation) and expressed as a product of the generalized (driving) force X_υ and rate $\dot{\chi}$, see Eq. (29). The force X_υ is the global dissipation increment due to SC only during the complete SC in the transforming region; the rate $\dot{\chi}$ is the reverse transformation time t_s, Eq. (30). Here m_n is the mass of transforming region, $\bar{X}$ is the driving force per unit mass and X is the volumetric part of the driving force, $\Delta\Gamma$ is the increment of the total surface energy of transforming volume.

Eqs. (31) and (32) represent the general expression for the volumetric part of the driving force, where φ is the mechanical contribution and we assumed for simplicity that the specific heat ν does not change during the SC. Then the increment of the thermal part of Helmholtz free energy is $\Delta\psi_\theta = \Delta s_0(\theta_0 - \theta_{ef})$, where Δs_o is the jump in reference values of entropy, θ is the temperature, θ_o is the equilibrium temperature which is determined from the condition that the jump in the thermal part of the Helmholtz free energy is zero at $\theta = \theta_0$, $\Delta\psi_\theta(\theta_0) = 0$. The effective temperature θ_{ef} is the temperature averaged over the transformation process and mass of the transforming region, see Eq. (33), where ρ is the mass density.

For PT and twinning we neglect the change in elastic moduli [Eqs. (34) and (35)] in this paper. For twinning additionally $\Delta s_0 = 0$ [Eq. (35)]. For the fracture transformation strain is absent [Eq. (36)].

The temperature evolution equation Eq. (37) in adiabatic approximation (see Levitas et al., 1998b; Levitas, 2000b) contains two heat sources, namely due to stress power and heat of SC.

As is usual in irreversible thermodynamics, the kinetic equation between force and rate $X_\upsilon = K_\upsilon(\dot{\chi}, \ldots)$ (or between rate and force which can be expressed in the form $t_s = F(X_\upsilon, \ldots)$) has to be given.

We will consider two types of SC kinetics:

- Athermal kinetics, for which K_υ is independent of the rate $\dot{\chi}$. In this case real time and rate do not play a part, SC occurs instantaneously when $\bar{X}$ reaches dissipative threshold K_0 [Eq. (38)].
- Time-dependent thermally activated kinetics. We assume that SC starts, when the driving force exceeds some threshold K^0, which is athermal part of the driving force, see Eq. (43) (at $\bar{X} - K^0 < 0\ \dot{\chi} = 0$). Following Levitas (1998b), we consider the size-dependent Arrhenius-type kinetics Eq. (44). Here E_a is the activation energy per unit mass at $\bar{X} - K^0 = 0$, R is the gas constant, t_o is some characteristic time, n is the number of atoms in volume V_n which undergo thermal fluctuations, N is the Avogadro's number. Last inequality in Eq. (44) means the positiveness of an actual activation energy $\bar{E}_a := E_a - \bar{X} + K^0$, otherwise the process does not need thermal activations. By introducing the effective temperature we also take into account the fact that temperature can vary significantly during the SC.

There are a lot of sources of athermal dissipation K^0 due to PT (Olson and Cohen, 1986):

1. Interaction of transformation strain or moving interface with various defects, e.g. point defects (solute and impurity atoms, vacancies), dislocations, grain, subgrain and twin boundaries and precipitates;
2. Emission of acoustic waves;
3. Crystal periodic resistance force (Peierls barrier).

The value K^0 can be different for nucleation and interface propagation, as well as for direct and reverse PT, and it seems to be a very complex functional of the thermomechanical deformation process and the material microstructure. At the same time in the papers by Levitas (1997, 1998a) the surprisingly simple formula (39) is obtained by comparison of some high pressure experiments with the solution of corresponding boundary-value problems assuming athermal kinetics, where $\bar{\sigma}_y$ is the current value of the yield stress averaged over the transforming region before PT, $3\varepsilon_o$ is the volumetric transformation strain, and L is the coefficient. The value L was determined by Levitas (1997) for some materials. The physical interpretation of Eq. (39) is as follows. The parameter K^0 characterizes an interaction of moving interface and material microstructure, and the yield stress is an integral characteristic of microstructure because plastic flow represents the motion of dislocations through the same obstacles (point, linear and other defects). If we assume the validity of Eq. (39) in the general case, then the dependence of K^0 on temperature, plastic strain, plastic strain rate and history, grain size and so on are determined. At large strains, according to the regularity revealed by Levitas (1996), σ_y and consequently K^0 have to be strain and strain-history independent.

Just by analogy we can assume a validity of the similar formula $K^0 = A\bar{\sigma}_y$ for twinning and fracture in plastic materials and try to find experimental arguments for this hypothesis in future.

2.5. Extremum principle for SC

In a general case the actual position, shape and orientation of volume V_n of a new transforming region, transformation strain and so on (which we designate by the vector of unknowns $\mathbf{b}$) in the SC criterion (38) or (43) and kinetic Eq. (44) are unknown. To determine them for time independent kinetics, we can use the extremum principle (40) which follows from the postulate of realizability (Levitas, 1995, 1998a), where $\mathbf{b}^*$ is the admissible value of the vector $\mathbf{b}$. The physical interpretation of the principle (40) is as follows: as soon as during the increase in the driving force the SC criterion (38) is fulfilled for the first time for some parameters $\mathbf{b}$, SC occurs with this $\mathbf{b}$. For all other $\mathbf{b}^*$ the inequality (40) is valid, because in the opposite case the SC criterion (38) will be met for this $\mathbf{b}^*$ earlier than for $\mathbf{b}$.

It is possible that under the given increment of boundary conditions the thermodynamic criterion of SC (38) and extremum principle (40) allow several solutions, e.g. transformation in different places, a solution with PT or fracture. At least two solutions are always possible when thermodynamic criterion of SC can be met: first, the solution with the SC, second, the solution without the SC, because all field and constitutive equations of continuum mechanics are satisfied. Such a situation was revealed in the papers by Levitas (1995) and Levitas et al. (1999) for PT. It was suggested that the best unique solution among all possible is the stable one. To formulate the stability criterion the postulate of realizability is again applied. Using it, the extremum principle for the whole volume is derived to choose the stable solution. The general extremum principle (Levitas, 1995) is too bulky. Here we will use the simplified versions (41) or (42) of this principle either at the prescribed displacements $\mathbf{u}$ or at a given traction vector $\mathbf{p}$ at the boundary S of volume V, where $\mathbf{u}_1$ and $\mathbf{u}_2$ correspond to the start and end of SC. It follows from principles (41) or (42) that the stable solution minimizes the work of external stresses at given displacements and maximizes the work of external stresses at prescribed tractions. Consequently, the fulfillment of the thermodynamic SC criterion is not sufficient for the occurrence of SC and only the extremum principle (41) or (42) which represents the global SC criterion yields the final solution.

For time dependent kinetics the postulate of realizability results in the principle of the minimum of transformation time (Levitas, 1998b,c), see Eq. (45). Let a characteristic size of nucleus not be determinable from principle Eq. (45) alone, because the thermodynamic criterion of SC is violated. Then the thermodynamic restriction $\bar{X}(\mathbf{b}^*) - K^0(\mathbf{b}) = 0$ has to be taken into account. Allowance for this constraint in Eq. (45) when E_a and θ_{ef} are independent of $\mathbf{b}^*$ results in the principle of the minimum of transforming mass (47) and a simplified kinetic Eq. (48).

Note that for fracture, extremum principles similar to those presented by Eqs. (41) and (42) are derived by Bazant (1989); analysis of the method of derivation is given by Levitas (1995).

Box 1. Field and constitutive equations

1. Kinematics

(a) Small strains
Linear decomposition of the total strain ε and the total strain rate $\dot{\varepsilon}$

$$\varepsilon := \left(\frac{\partial \mathbf{u}}{\partial \mathbf{r}}\right)_s = \varepsilon_e + \varepsilon_p + \varepsilon_t, \tag{6}$$

$$\dot{\varepsilon} := \left(\frac{\partial \mathbf{v}}{\partial \mathbf{r}}\right)_s = \dot{\varepsilon}_e + \mathbf{d}_p + \dot{\varepsilon}_t, \quad \mathbf{d}_p = \dot{\varepsilon}_p. \tag{7}$$

$$\text{Accumulated plastic strain} \quad \dot{q} := (2/3\mathbf{d}_p : \mathbf{d}_p)^{1/2}. \tag{8}$$

The dimensionless order parameter ξ

$$\xi := \frac{|\varepsilon_t|}{|\varepsilon_{t2}|} \text{ for PT and twinning,} \tag{9}$$

$$\xi := 1 - \frac{E}{E_1} = 1 - \frac{\sigma_y}{\sigma_{y1}} \text{ for fracture.} \tag{10}$$

The transformation strain ε_t

$$\varepsilon_t = \xi \varepsilon_{t2}, \quad \xi \in [0, 1] \tag{11}$$

(b) Finite strains
Multiplicative decomposition of the total deformation gradient $\mathbf{F}$

$$\mathbf{F} = \frac{\partial \mathbf{r}}{\partial \mathbf{r}_\tau} = \mathbf{F}_e \cdot \mathbf{F}_t \cdot \mathbf{F}_p = \mathbf{V}_e \cdot \mathbf{R}_e \cdot \mathbf{F}_t \cdot \mathbf{F}_p. \tag{12}$$

The elastic strain tensor $\mathbf{B}_e$

$$\mathbf{B}_e := 0.5(\mathbf{F}_e \cdot \mathbf{F}_e^t - \mathbf{I}) = 0.5(\mathbf{V}_e \cdot \mathbf{V}_e - \mathbf{I}) \approx \varepsilon_e \ll \mathbf{I}. \tag{13}$$

The dimensionless order parameter ξ

$$\xi := \frac{|\mathbf{F}_t - \mathbf{I}|}{|\mathbf{F}_{t2} - \mathbf{I}|} \text{ for PT and twinning,} \tag{14}$$

$$\xi := 1 - \frac{E}{E_1} = 1 - \frac{\sigma_y}{\sigma_{y1}} \text{ for fracture.} \tag{15}$$

The transformation gradient $\mathbf{F}_t$

$$\mathbf{F}_t = \mathbf{I} + \xi(\mathbf{F}_{t2} - \mathbf{I}), \quad \xi \in [0, 1] \tag{16}$$

Decomposition of the total deformation rate $\mathbf{d}$

$$\mathbf{d} := \left(\frac{\partial}{\partial \mathbf{r}}\right)_s = (\dot{\mathbf{F}}_e \cdot \mathbf{F}_e^{-1})_s + \mathbf{d}_t + \mathbf{d}_p, \tag{17}$$

$$\mathbf{d}_p := (\mathbf{F}_e \cdot \mathbf{F}_t \cdot \dot{\mathbf{F}}_p \cdot \mathbf{F}_p^{-1} \cdot \mathbf{F}_t^{-1} \cdot \mathbf{F}_e^{-1})_s = \mathbf{F}_e \cdot \mathbf{F}_t \cdot \dot{\mathbf{F}}_p \cdot \mathbf{F}_p^{-1} \cdot \mathbf{F}_t^{-1} \cdot \mathbf{F}_e^{-1}, \tag{18}$$

$$\mathbf{d}_t := (\mathbf{F}_e \cdot \dot{\mathbf{F}}_t \cdot \mathbf{F}_t^{-1} \cdot \mathbf{F}_e^{-1})_s = (\mathbf{F}_e \cdot (\mathbf{F}_{t2} - \mathbf{I}) \cdot \mathbf{F}_t^{-1} \cdot \mathbf{F}_e^{-1})_s \dot{\xi}. \tag{19}$$

$$\text{Accumulated plastic strain } \dot{q} := (2/3 \mathbf{d}_p : \mathbf{d}_p)^{1/2}. \tag{20}$$

2. Constitutive equations

$$\text{Hooke's law} \quad \mathbf{T} = \mathbf{E} : \varepsilon_e = K I_1(\varepsilon_e)\mathbf{I} + 2G dev \varepsilon_e. \tag{21}$$

$$\text{Yield function} \quad f(\mathbf{T}, q, \xi) = \sigma_i - \sigma_y(q, \xi) \leqslant 0. \tag{22}$$

$$\text{Plastic flow rule} \quad \mathbf{d}_p = \lambda \mathbf{s}. \tag{23}$$

$$\text{The Kuhn} - \text{Tucker conditions} \quad f(\mathbf{T}, q, \xi) \leqslant 0, \lambda \geqslant 0, \lambda f(\mathbf{T}, q, \xi) = 0. \tag{24}$$

3. Equilibrium equations

$$\nabla \cdot \mathbf{T} = 0.$$

4. Sliding condition at the interface

$$|\tau_n| < \tau_c \Rightarrow \mathbf{u}^2 - \dot{\mathbf{u}}^1 = 0 \quad \text{(coherent interface)}, \tag{25}$$

$$|\tau_n| = \tau_c \Rightarrow \dot{\mathbf{u}}_\tau^2 - \dot{\mathbf{u}}_\tau^1 = \lambda_1 \tau_n, \quad \dot{u}_n^2 - \dot{u}_n^1 = 0, \quad \lambda_1 \geqslant 0 \quad \text{(incoherent interface)}. \tag{26}$$

5. Decohesion condition at the interface

$$\sigma_n < \sigma_c \Rightarrow \dot{\mathbf{u}}^2 - \dot{\mathbf{u}}^1 = 0, \tag{27}$$

$$\sigma_n = \sigma_c \Rightarrow \dot{\mathbf{u}}^2 - \dot{\mathbf{u}}^1 \neq 0, \quad \sigma_n = 0, \tau_n = 0, \tag{28}$$

Box 2. Equations for structural changes in some transforming region

1. Definitions

Dissipation rate due to SC

$$\mathcal{D}_\xi = X_\upsilon \dot{\chi}, \tag{29}$$

$$\frac{X_\upsilon}{m_n} := \bar{X} := X - \frac{1}{m_n} \Delta \int_{\Sigma_n} \Gamma \mathrm{d}\Sigma_n, \quad \dot{\chi} := \frac{1}{t_s} \tag{30}$$

General expression for the driving force

$$X := \varphi - \Delta s_0 (\theta_0 - \theta_{ef}), \tag{31}$$

$$\varphi := \frac{1}{m_n}\int_{V_n}\left(\int_0^1 \mathbf{T} : \mathbf{d}_t \frac{dt}{d\xi} d\xi - \frac{1}{2}\int_{\mathbf{E}_1}^{\mathbf{E}_2} \varepsilon_e : d\mathbf{E} : \varepsilon_e\right) dV_n. \tag{32}$$

Effective temperature

$$\theta_{ef} = \frac{1}{m_n}\int_{V_n}\int_0^1 \rho\theta d\xi dV_n. \tag{33}$$

Phase transformation $(\Delta\mathbf{E} = 0)$

$$\varphi = \frac{1}{m_n}\int_{V_n}\int_0^1 \mathbf{T} : \mathbf{d}_t \frac{dt}{d\xi} d\xi dV_n. \tag{34}$$

Twinning $(\Delta\mathbf{E} = 0, \Delta s_0 = 0)$

$$X = \varphi = \frac{1}{m_n}\int_{V_n}\int_0^1 \mathbf{T} : \mathbf{d}_t \frac{dt}{d\xi} d\xi dV_n. \tag{35}$$

Fracture $(\mathbf{F}_{t2} = \mathbf{I})$

$$\varphi = -\frac{1}{2m_n}\int_{V_n}\int_{\mathbf{E}_1}^0 \varepsilon_e : d\mathbf{E} : \varepsilon_e dV_n. \tag{36}$$

2. Temperature evolution for adiabatic SC-processes

$$v\dot{\theta} = \frac{1}{\rho}\mathbf{T} : \mathbf{d} - \Delta s_0 \theta_0 \dot{\xi}. \tag{37}$$

3. Constitutive equations

(a) Time-independent kinetics
SC criterion

$$\bar{X} = K^0. \tag{38}$$

Dissipative threshold K^0 for phase transformation

$$K^0 = 3L\bar{\sigma}_\gamma\varepsilon_o. \tag{39}$$

Extremum principle for SC

$$\bar{X}(\mathbf{b}^*) - K^0(\mathbf{b}^*) < 0 = \bar{X}(\mathbf{b}) - K^0(\mathbf{b}). \tag{40}$$

Extremum principle for the determination of a stable solution (global SC criterion)

$$\int_S \int_{\mathbf{u}_1}^{\mathbf{u}_2} \mathbf{p}\cdot \mathrm{d}\mathbf{u}\mathrm{d}S \;\Rightarrow\; \min \tag{41}$$

(a particular case at prescribed $\mathbf{u}$ at S).

$$\int_S \int_{\mathbf{u}_1}^{\mathbf{u}_2} \mathbf{p}\cdot \mathrm{d}\mathbf{u}\mathrm{d}S \;\Rightarrow\; \max \tag{42}$$

(a particular case at prescribed $\mathbf{p}$ at S)
(b) Thermally activated kinetics
SC criterion

$$\bar{X} \geqslant K^0. \tag{43}$$

Kinetic equation

$$t_\mathrm{s} = t_\mathrm{o}\exp\left(-\frac{\left(\bar{X} - K^0 - E_\mathrm{a}\right)m_\mathrm{n}}{R\theta_\mathrm{ef}}\frac{N}{n}\right) \quad \text{at} \quad 0 \leqslant \bar{X} - K^0 \leqslant E_\mathrm{a}. \tag{44}$$

Principle of minimum of transformation time

$$t_\mathrm{s} = t_\mathrm{o}\exp - \frac{\left(\bar{X}(\mathbf{b}^*) - K^0(\mathbf{b}^*) - E_\mathrm{a}(\mathbf{b}^*)\right)m_\mathrm{n}^*}{R\theta_\mathrm{ef}^*}\frac{N}{n} \;\rightarrow\; \min. \tag{45}$$

Principle (45) under thermodynamic constraint

$$\bar{X}(\mathbf{b}^*) - K^0(\mathbf{b}^*) = 0 \tag{46}$$

at E_a and θ_ef independent of $\mathbf{b}^*$, namely the principle of the minimum of transforming mass

$$m_\mathrm{n}^* \;\rightarrow\; \min. \tag{47}$$

Simplified kinetic equation

$$t_\mathrm{s} = t_\mathrm{o}\exp\left(\frac{E_\mathrm{a}m_\mathrm{n}}{R\theta_\mathrm{ef}}\frac{N}{n}\right). \tag{48}$$

3. Numerical method

For time dependent kinetics a general scheme for the application of SC criterion (43), kinetic Eq. (44) and extremum principle (45), as well as the temperature evolution Eq. (37) is as follows. All the material properties and constitutive equations must be given for each intermediate state of SC, i.e. for $\xi \in [0,1]$. Then we assume that at some prescribed initial and boundary conditions some SC occurs in some region V_n. We introduce the transformation strain and change the material properties from initial to final values incrementally in a possible SC region. After solving the elastoplastic and thermal boundary-value problems for each step we determine the variation of all the fields, calculate the driving force $\bar{X}$ and resistance K^0 and at $\bar{X} - K^0 \geqslant 0$ determine the SC time t_s from Eq. (44) or (48). Then we vary the possible SC region and way of varying the transformation strain and properties from initial to final values in it and find such a SC region and the way of varying the transformation strain and properties which minimize the transformation time. For time independent kinetics the procedure is as follows. In the same way as for time dependent kinetics we determine $\bar{X} - K^0$ for the chosen SC region. Then we vary the possible SC region (and way of varying the transformation strain and properties from initial to final values in it) and find such an SC region which maximizes the difference $\bar{X} - K^0$, see Eq. (40). Then the SC starting temperature θ_s, or the increment of boundary conditions or initial conditions are determined from the SC criterion $\bar{X} - K^0 = 0$.

It is necessary to note that in our numerical approach we consider 'inverse' problems, i.e. instead of a 'direct' problem of determining the transforming region at some variation in temperature or (and) boundary conditions we solve a set of 'inverse' problems for which the position and the size of the transforming region (nucleus) and the way of varying the transformation strain and material properties in it are prescribed in advance.

In our concrete problems the way of varying the transformation strain and properties from initial to final values is fixed. In particular, the transformation deformation gradient varies homogeneously in the transforming region according to Eq. (16) for PT and twinning, for fracture Young's modulus E, and the yield stress σ_y decrease homogeneously in the transforming region proportionally to ξ [see Eq. (15). The temperature during PT is assumed to be homogeneous and fixed, or an adiabatic process holds.

We do not present here the numerical algorithm developed which is described in detail in the paper by Levitas et al. (1998a) for small strains and in the paper by Idesman et al. (1997b, 1999a,b) for finite strains for PT and twinning. We note only its main characteristic features. As a fracture in our approach is treated as a particular case of PT, then for fracture and PT we use the same numerical algorithm. For spatial discretization FEM is used (quadratic triangular finite elements are used for all the model problems considered below).

1. In order to calculate the variation of stress-strain state during PT or twinning or for fracture, we have to solve an elastoplastic problem incrementally with the

prescribed transformation deformation gradient $\mathbf{F}_t$ (or with the transformation strain ε_t at small strains) for PT and twinning or with the decreasing Young's modulus and yield stress in the region where fracture is assumed to occur. Such a formulation for SC is kinematically similar to the problem of thermoplasticity with anisotropic thermal expansion, i.e. the order parameter ξ can be treated like the temperature and the transformation deformation gradient (or the transformation strain at small strains) like the thermal deformation gradient (or the thermal strain at small strains). At small strains such a problem for PT is solved by the well-known numerical algorithms for thermoelastoplasticity in all the works on PT which were available to the authors (see for example Ganghoffer et al., 1991; Marketz and Fischer, 1994a,b; Reisner et al., 1998; Levitas et al., 1998a and others). At finite strains an extension of the algorithms based on the multiplicative decomposition of the deformation gradient was proposed in a paper by Idesman et al. (1999b) for the case with PT and twinning. The use of the current configuration and the true Cauchy stresses along with assumptions of small elastic strains and the condition of zero modified plastic spin allows us to apply the radial return algorithm and to derive quite a simple formula for the consistent elastoplastic moduli. Some modifications of the iterative algorithm related to the numerical integration of constitutive equations along with the radial return algorithm are suggested in order to improve the accuracy of solutions for large increments in external load (such modifications can be used for any elastoplastic problem without SC as well). A similar approach will be applied in this paper to fracture as well.

2. A proposed simple model for an incoherent interface and interface with decohesion [see Eqs. (25)–(28)] prescribes the special conditions at the interfaces between parent and product phases. Mathematically these conditions are equivalent to the usual contact conditions for elastoplastic problems. To solve a contact problem we use a numerical algorithm proposed by Idesman and Levitas (1995) which includes the combination of iterative cycles to allow for incoherence (decohesion) and plastic deformation. In finite element discretization the pair of nodes with the same coordinates are introduced at the interfaces.
3. The simplest approach to solving the extremum problem for the determination of PT regions is given by Levitas et al. (1998a) for small strains and time independent kinetics. A similar method can be used for finite strains and time dependent kinetics as well. It includes checking the set of regions for the possibility of SC and the choice of the most favorable one according to the extremum principle. But unfortunately such a procedure requires huge computation time and additional investigations regarding the mesh dependency of the solutions obtained. Here we will use a simplified method to find a "constrained" solution. The shape of the transforming regions (in our case rectangular) is assumed and the geometric parameters of the transforming regions and (or) their sequence will be found as a solution of the corresponding extremum problem.

4. Numerical study of phase transformations and twinning in elastoplastic materials

The following presumptions hold for the problems considered below.

(a) For PT the volumetric transformation strain is small, and the mass densities ρ for the parent and product phases are approximately the same.
(b) Elastic properties of the product and parent phases for all the problems considered are the same: Young's modulus $E = 2 \cdot 10^5$ MPa, Poisson ratio $\nu_o = 0.3$.

4.1. Progress of PT (layer by layer) in a cylindrical sample

Axisymmetric problems for the sequence of PT layers prescribed in advance with the coherent and incoherent interfaces and time independent kinetics were studied in the papers by Idesman et al. (1997a) and Levitas et al. (1998a). Here we consider another formulation. Fig. 2 shows a cylindrical sample. The half of its cross-section is subdivided into 5 layers in which PT can occur. The following assumption is made for the PT calculation: PT occurs at any time instant in one layer only. For this state, the whole deformation process of PT in the layer has to be computed. Every layer is considered as a possible new nucleus. Only after finishing PT in one layer can PT start in another one.

The following boundary conditions are applied:

- along CD and DE boundaries $u_n = 0$, $\tau_n = 0$;

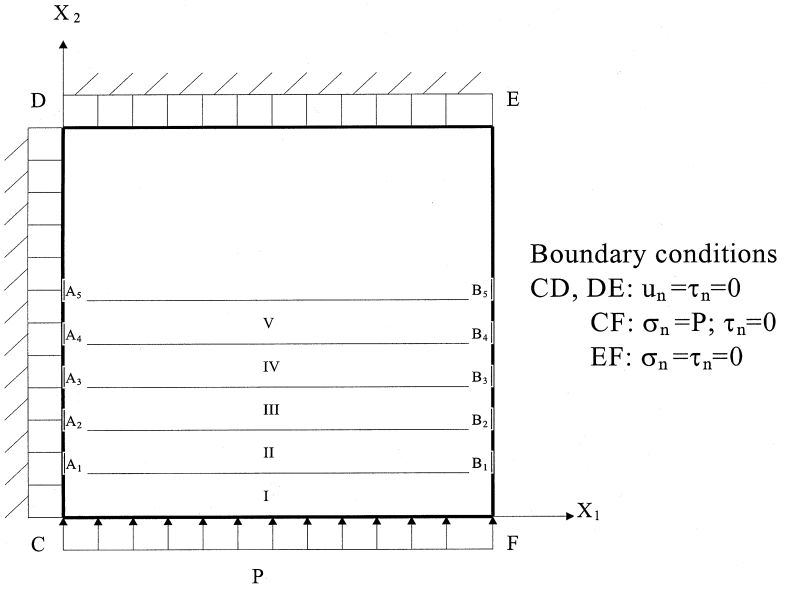

Fig. 2. Half of the cross-section of a cylindrical sample with layers I–V, where PT can occur.

- along EF boundary $\sigma_n = \tau_n = 0$ (free surface);
- along CF boundary $\sigma_n = P$, $\tau_n = 0$,

where u_n is the normal displacement, τ_n is the tangential stress, σ_n is the normal stress, P is the prescribed fixed compressive stress P (we study two cases with $P = 100$ and 180 MPa). The new phase is assumed to be elastic at once after beginning of PT. The following two cases of the plastic properties of the matrix are considered: (a) a perfect elastoplastic material with the yield stress $\sigma_y = 180$ MPa; (b) an elastoplastic material with isotropic hardening $\sigma_y = 250 + 2000$ q MPa.

The PT in a layer is simulated by an increase in the compressive volumetric transformation strain ε_o from 0 to the final value -0.01 with increment $|\varepsilon_o| = 0.002$ (the dilatational PT is considered). PT is initiated by homogeneous variation of temperature. During PT the temperature is assumed to be fixed and its value is determined from the PT criterion.

First let us analyze the results obtained by Idesman et al. (1997a) and Levitas et al. (1998a). It appears that the coherent interface in an elastic material at $K^0 = \text{const}$ is unstable, i.e., if PT occurs in the first layer, then, at the same temperature and external stresses, PT should occur in all the remaining layers, because the transformation work φ grows. To describe the stable phase equilibrium we should assume heterogeneous distribution of K^0 or growing K^0 with increasing volume fraction c of the new phase.

It is assumed for an incoherent interface in the elastic matrix that after completing the PT in the layer the displacement discontinuities at the layer interface do not change. This corresponds to the frozen surface dislocations. The incoherence stimulates PT significantly in the first layer (φ increases). The mechanical part of the driving force φ in the second layer for an incoherent interface is smaller than for a coherent interface, but a little larger than for the first layer with the incoherent interface. That is why at $K^0 = \text{const}$ or for slightly growing $K^0(c)$ an incoherent PT in the second layer can occur at once after PT in the first layer under the same external conditions. The value φ for incoherent PT in the third layer is smaller than in the first and second layer and much smaller than in the third layer for coherent PT. If the value $K^0(c)$ is large enough to stop the coherent interface motion with fixed external parameters after PT in layers 2-4 ($\varphi \simeq 0$ MPa), then it is necessary to change the external parameters very significantly in order to shift the incoherent interface ($\varphi \simeq -12$ MPa). With such changes in external parameters PT can occur at other places in a sample, which leads to the formation of a discrete microstructure. The results of the computation explain the known experimental facts that an incoherent interface has low mobility or cannot move at all. The reason for the decreasing value of φ for an incoherent interface is the change in internal stresses.

A plastic deformation of the matrix acts in the same way as incoherence: it promotes nucleation, the PT in the second layer occurs immediately after PT in the first layer under the same external conditions. For PT in 3–5 layers it is necessary to change the external condition in order to enforce PT, i. e. due to plasticity it is possible to obtain a stable interface motion.

In the given paper we study the application of the extremum principle (40) to the computation of PT regions. We consider various values of the external force P and

materials with various plastic properties of the matrix. The interface between the parent and product phases is assumed to be coherent.

The following algorithm is used for the determination of the PT region. First of all we consider PT in each of 5 layers (5 independent problems), calculate the driving force and the threshold for each layer and choose the layer with the maximum value $\bar{X} - K^0$. If K^0 is a constant, then the layer corresponding to the maximal driving force is chosen. In this layer PT occurs first of all according to the extremum principle for PT (40). In order to determine the next transforming layer, each of the remaining 4 layers is considered as a possible PT region and the procedure of searching for the next layer with PT is repeated. In this way we can calculate PT progress in all the layers. The local stress and strain fields in the sample appeared after PT in the transformed layers are used as the initial data for the solution of the next layer. The finite element mesh with refinement in transforming layers is shown in Fig. 3.

The results of the calculations presented in Figs. 4–10 show that different combinations of external conditions and elastoplastic properties are responsible for the formation of different microstructures. At $P = 100$ MPa, $\sigma_y = 180$ MPa and constant K^0 the calculated mechanical part φ of the driving forces presented in Fig. 4 determines the formation of a discrete microstructure, Fig. 5. At first PT occurs in the first layer for which the value $\varphi = -5.2$ MPa is the largest among all the 5 layers (see the first 5 columns in Fig. 4). Then PT occurs in the 3rd and the 5th layers for which

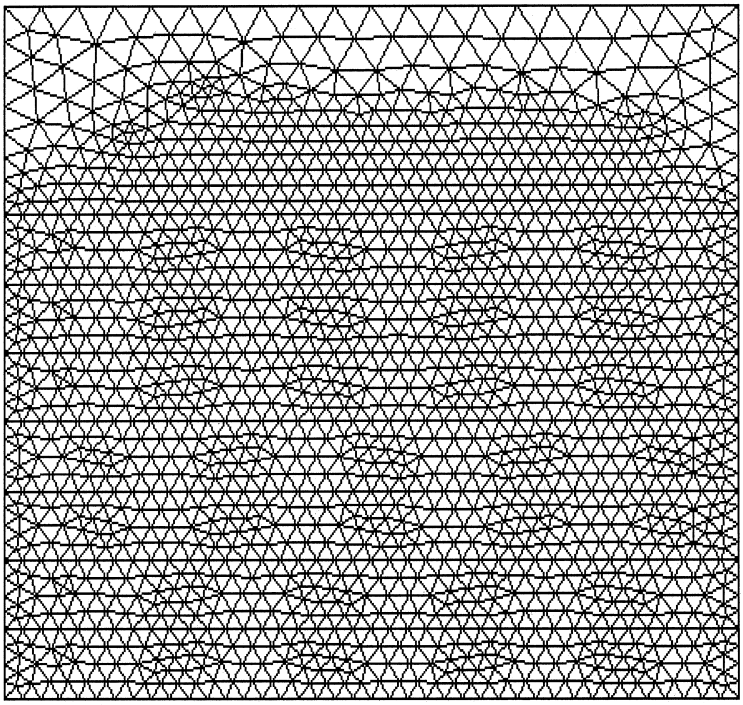

Fig. 3. Finite element mesh with refinement in transforming layers.

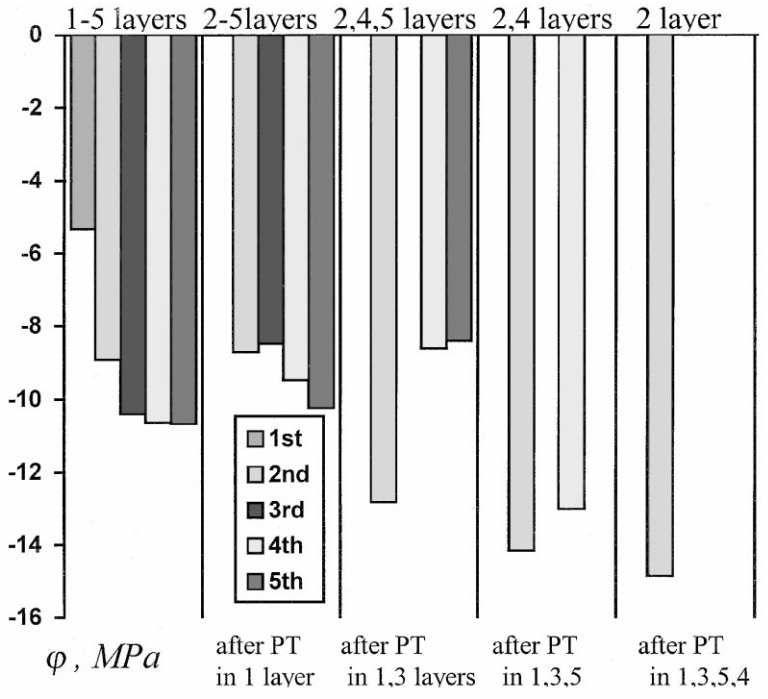

Fig. 4. Values of the transformation work φ for each layer for PT at $P = 100$ MPa and $\sigma_y = 180$ MPa.

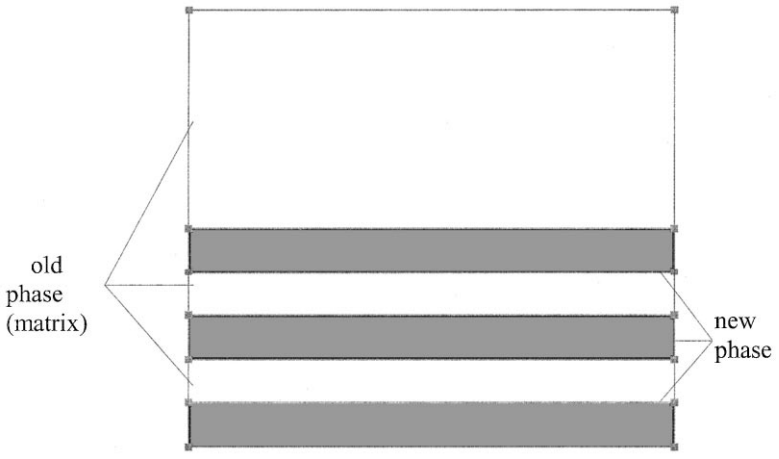

Fig. 5. A discrete microstructure obtained during PT at $P = 100$ MPa and $\sigma_y = 180$ MPa.

the value φ is the largest among the remaining 4 and 3 layers respectively (see the second 4 columns and the third 3 columns in Fig. 4). Finally, PT in the fourth and then in the second layer occurs. The progress of PT is accompanied by a decreasing mechanical part of the driving force φ from -5.2 MPa for the first layer to -12.9

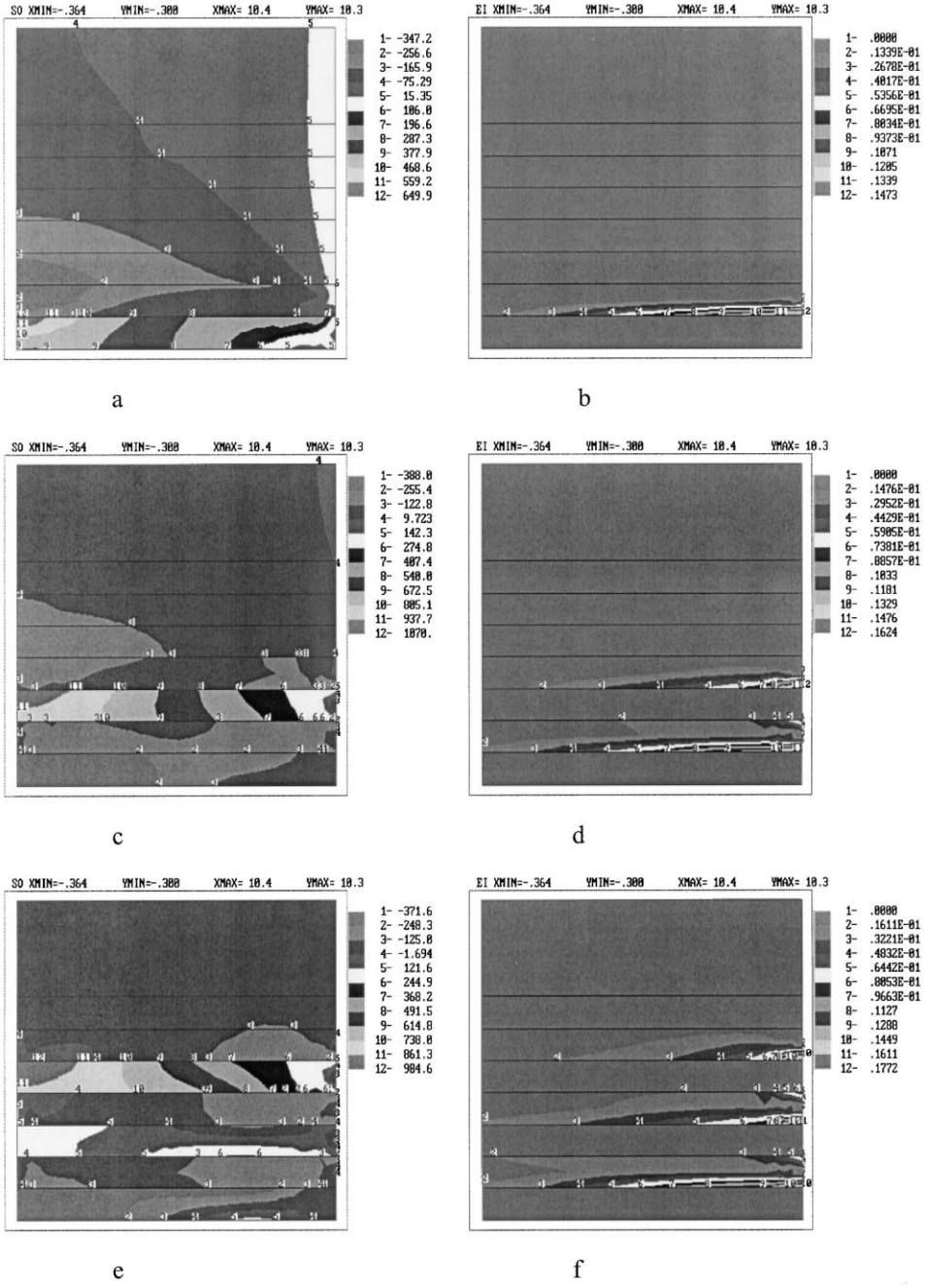

Fig. 6. The distribution of pressure (a,c,e) and equivalent plastic strain (b,d,f) in the sample after PT in 1st (a,b), 1st and 3rd (c,d), 1st, 3rd and 5th (e,f) layers.

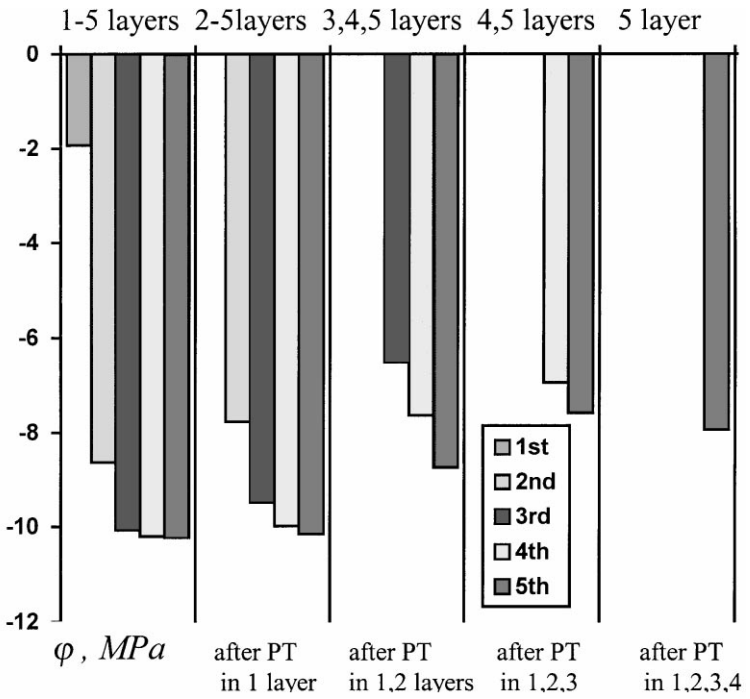

Fig. 7. Values of the transformation work φ for each layer during PT at $P = 180$ MPa and $\sigma_y = 180$ MPa.

MPa for the third layer, which requires considerable variation in temperature for the PT progress. In Fig. 6 the distribution of pressure and equivalent plastic strain during PT progress is shown. The stress and strain fields in regions where PT have already occurred affect the PT condition in new regions.

The solution of the problem for $P = 180$ MPa and $\sigma_y = 180$ MPa presented in Figs. 7 and 8 demonstrates another scenario of PT progress, namely, the subsequent PT in layers occurs, i.e. after the first layer PT occurs in the second one, then in the third layer and so on. Such a PT progress corresponds to motion of the coherent interface, see also Idesman et al. (1997a).

One possible reason for the formation of a discrete microstructure for a plastically hardening material is related to the linear dependence of K^0 on yield stress $\bar{\sigma}_y$, averaged over the transforming layer at the beginning of PT, see Eq. (39), where the value L is equal to 7.48 for steel (see Levitas, 1997). For linear hardening materials it is equivalent to the linear dependence of $K^0(\bar{q})$ on the accumulated plastic strain $\bar{q}$, averaged over the transforming layer at the beginning of PT ($K^0(\bar{q}) = K_0^0 + \Delta K^0(\bar{q})$, $\Delta K^0(\bar{q}) = a\bar{q}$, where K_0^0 and a are the material constants). The results of the problem for a hardening elastoplastic matrix with $\sigma_y(q) = 250 + 2000\ q$ and $P = 100$ MPa are given in Figs. 9 and 10. Without allowing for the dependence of $K^0(\bar{q})$ on accumulated plastic strain $\bar{q}$ the subsequent PT in layers occurs (see Fig. 9), i.e. after the first layer PT occurs in the second one, then in the third layer and so on. Allowing for this dependence the formation of the discrete microstructure (see Fig.

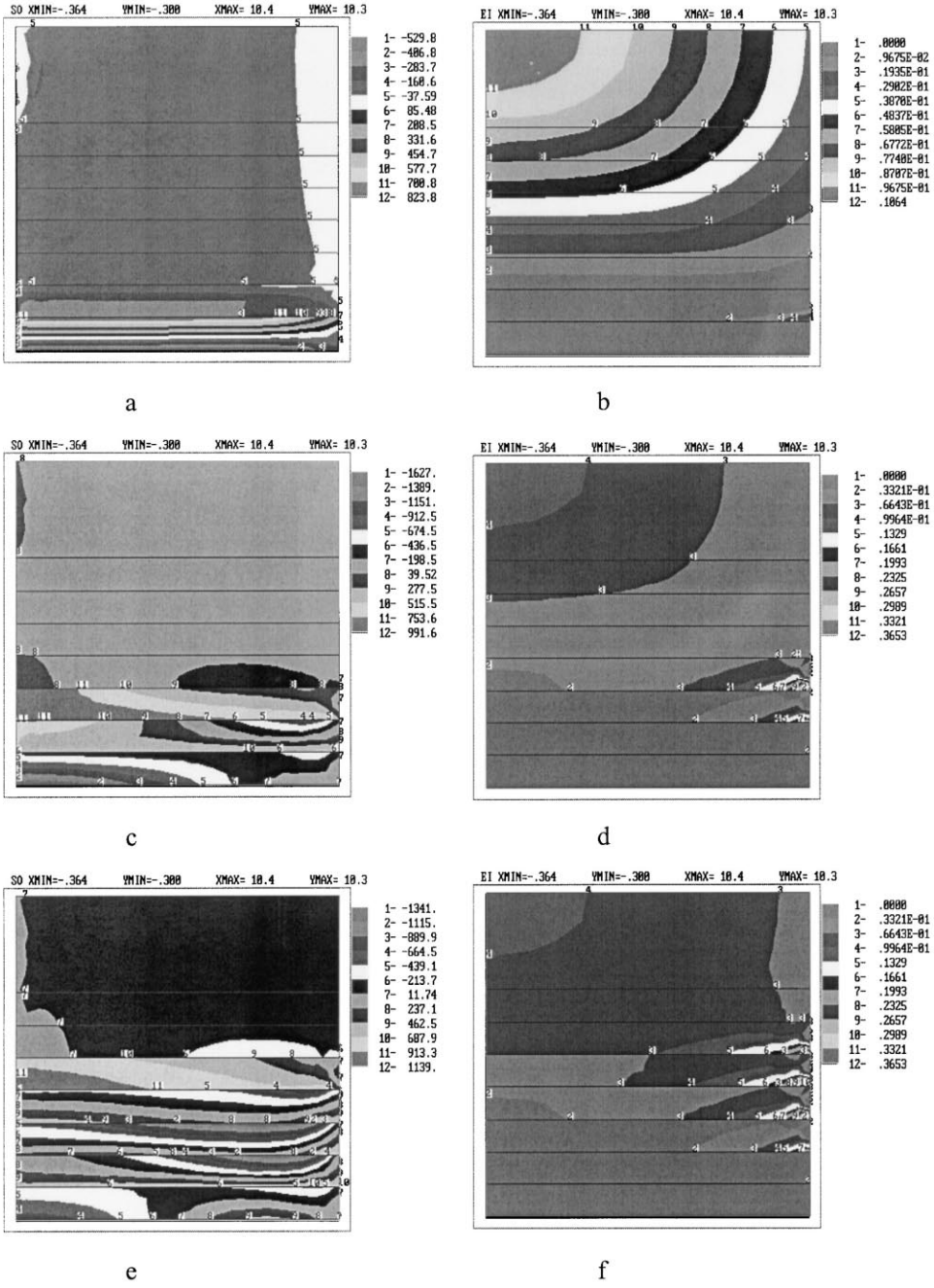

Fig. 8. The distribution of pressure (a,c,e) and equivalent plastic strain (b,d,f) in the sample after PT in 1st (a,b), 1st, 2nd and 3rd (c,d), 1st, 2nd, 3rd, 4th and 5th (e,f) layers.

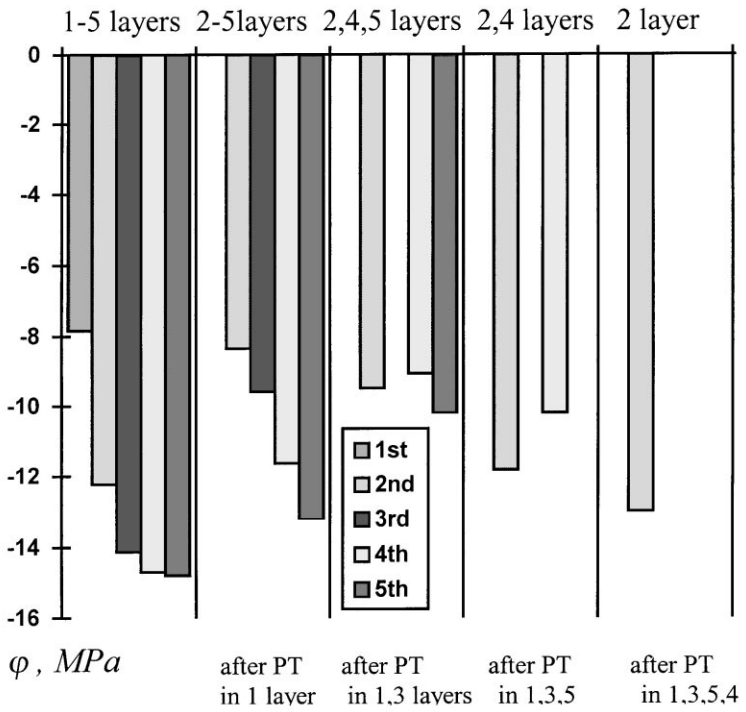

Fig. 9. Values of the transformation work φ for each layer for PT at P = 250 + 2000 q.

10) occurs as in Fig. 5. Consequently, for the general case of the variable K^0 the simplified approach based on maximization of the transformation work φ leads to wrong results. Application of the more general extremum principle (40) derived with the help of postulate of realizability is required.

As plastic deformations are concentrated near the interface and decay with growing distance from the interface, the value K^0 decays when moving away from the interface. Strain hardening in the layer next to the transforming one suppresses the subsequent PT in it. In fact, the plastic strain field in Fig. 6 determines the natural spacing between transforming regions if it is varied.

4.2. Adiabatic nucleation at shear-band intersection

It is known from experiments (see Olson and Cohen, 1972; Olson, 1984; Stringfellow et al., 1992) that

- shear-band intersections are the major nucleation sites;
- growth beyond the intersection region is generally very restricted;
- transformation occurs during the intersection events;
- transformation does not occur at every shear-band intersection.

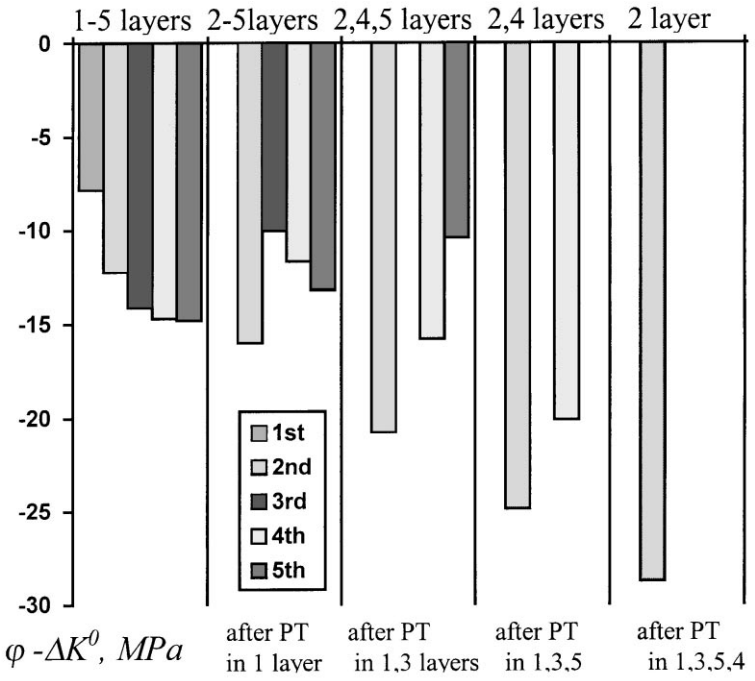

Fig. 10. Values of the expression $\varphi - \Delta K^0$ for each layer for PT at $P = 100$ MPa and $\sigma_y = 250 + 2000$ q.

The mechanical formulation and the solution of a model problem of nucleation at shear bands at a fixed homogeneous temperature and $K^0 = \text{const}$ are described by Idesman et al. (1999b) and in more detail by Levitas et al. (1999). Let us summarize the results reported in the last paper. It was demonstrated that for strain-induced transformation at shear-band intersections the transformation work is maximal in comparison with other possible locations, i.e. shear-band intersection is in fact the most favorable nucleation place. Further growth of the nucleus beyond the intersection is inhibited, because the transformation work decreases significantly and transformation at other shear-band intersections is favored. The higher transformation work explains also why PT is favored during the intersection event rather than after intersection and cooling at fixed stress. Transformation work depends strongly on the number of active shear-band intersections at the prescribed macroscopic strain increment. This favors sequential transformation at multiple intersections, even when the intersections are completely equivalent. At a given temperature, the necessary transformation work is determined from the PT criterion, and the number of active intersections is obtained using the numerical solution.

Hence, all four experimental observations enumerated above can be at least qualitatively described in the framework of continuum thermomechanics without detailed physical mechanisms. Of course, this does not diminish the role of concrete micromechanisms of interaction of PT and plasticity. An important point is that there are pure macroscopic (mechanisms-independent) reasons for the above phenomena,

and that each microscopic mechanism has to be checked from point of view of continuum thermodynamics.

Further, the relevance of stability analysis for strain-induced PT has been demonstrated. According to the stability criterion (41), when the macroscopic $\sigma - \varepsilon$ curve for the solution with PT exceeds the $\sigma - \varepsilon$ curve for the solution without PT, the PT will not occur, even when the local PT criterion can be satisfied. We will illustrate this in more detail for the next problem.

Calculations also demonstrate a large difference between PT conditions for displacement and stress controlled boundary conditions. For given fixed external stresses martensite growth increases the macroscopic axial strain and the transformation work, favoring growth beyond the intersection region, in contrast to the restricted growth predicted under displacement control. Maximum transformation work corresponds to the case when the whole band transforms into the martensitic state without plastic straining and is equal to the total work of the applied stress. Consequently, in stress controlled experiments shear band intersection is not the best place for nucleation. A plate-like nucleus is more favorable. These results are in line with experiments.

In a shear band and at the shear-band intersection an adiabatic heating is expected which can significantly change thermodynamic and kinetic conditions for PT. Here we consider the adiabatic formulation of a PT problem. The cross section of a sample for the case of a plane strain state is given in Fig. 11. The following

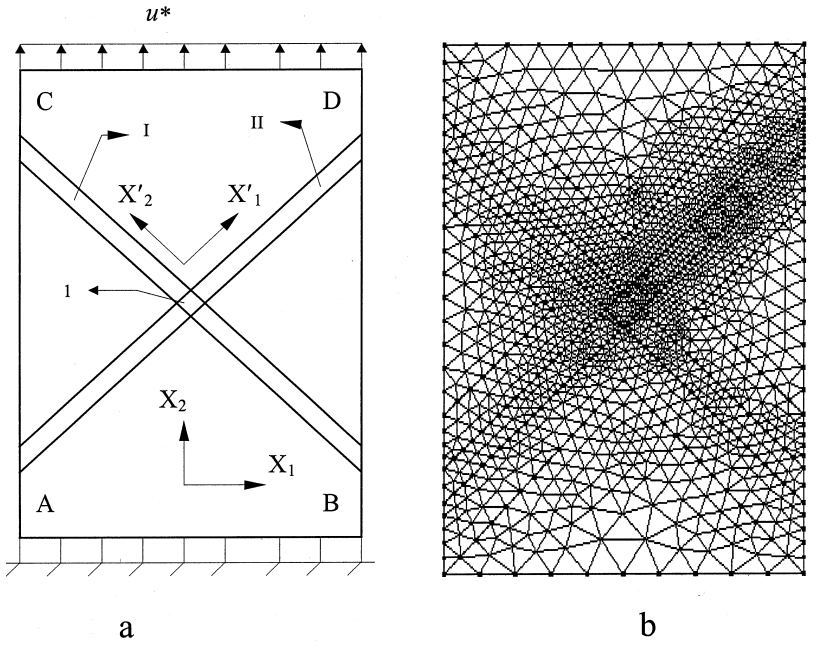

Fig. 11. Cross-section (a) and FE mesh (b) of a sample with a martensitic nucleus 1 at the intersection of two shear-bands (I and II).

assumptions hold: shear bands are introduced in advance; the material deforms elastoplastically within shear bands and elastically only outside shear bands; the nucleus appears at the shear-band intersection in the region I. The following thermomechanical properties of steel are used in calculations: yield stress $\sigma_y^m = 250$ MPa for an austenitic matrix (the nucleus is assumed to be elastic at once after beginning of PT); $\rho = 7.8 \cdot 10^{-9}$ Ns^2/mm^4, $\Delta s_0 = -11.6 \cdot 10^7$ mm^2/Ks^2, $\nu = 0.46 \cdot 10^9$ mm^2/Ks^2, $K^0 = 11.3 \cdot 10^9$ mm^2/s^2, $\theta_0 = 440$ K.

The following boundary conditions apply:

- along AB boundary, $u_n = 0$, $\tau_n = 0$;
- along CD boundary, $u_n = u^*_{max} = 0.24$, $\tau_n = 0$ (u^*_{max} is the prescribed normal displacement);
- along AC and BD, boundaries $\sigma_n = \tau_n = 0$ (free surface).

The transformation deformation gradient $\mathbf{F}_{t2}$ and the order parameter ξ are subdivided into 60 increments for calculations. In the local cartesian coordinate system (axes X'_1 and X'_2 are directed along shear bands, axis X_3 is orthogonal to them) the transformation deformation gradient $\mathbf{F}_{t2}$ has the following components

$$(F_{t2})_{11} = 1, (F_{t2})_{12} = 0.2, (F_{t2})_{21} = 0, (F_{t2})_{22} = 1.026, (F_{t2})_{33} = 1, \tag{49}$$

and the other components are zero.

We assume that during the PT not only the transformation deformation gradient, but also the prescribed displacements grow proportionally to the order parameter ξ,

$$u^*(\xi) = u^*_1 + (u^*_{max} - u^*_1)\xi, \tag{50}$$

which means that the transformation deformation gradient grows proportionally to the prescribed displacement. We start PT at $\varepsilon = \frac{u^*_1}{AC} = 0.14\%$, when plastic strains appear in shear-band regions. This corresponds to the situation where transformation occurs during the shear-band intersection event. As initial conditions we assume that at the beginning of PT the temperature is homogeneous and equal to the transformation starting temperature θ_s.

The temperature in the nucleus during adiabatic PT can be represented as

$$\theta = \theta_s + \Delta\theta, \tag{51}$$

where $\Delta\theta(\xi)$ [according to (37)] is equal to

$$\Delta\theta(\xi) = \frac{1}{\rho\nu}\int_0^\xi \mathbf{T} : \mathbf{d}_t \frac{dt}{d\xi} d\xi dV_n - \frac{\Delta s_0 \theta_0 \xi}{\nu}. \tag{52}$$

Then allowing for Eqs. (33), (51), (52) the PT starting temperature θ_s can be calculated from the PT criterion (38)

$$\varphi - \Delta s_0(\theta_0 - \theta_s + \frac{\rho}{m_n}\int_{V_n}\int_0^1 \Delta\theta \frac{dt}{d\xi} d\xi) = K^0. \tag{53}$$

The value of φ and the integral in Eq. (53) are calculated based on the finite element solution.

Remark. *In fact, we assumed that the PT starting temperature is* $\theta_s = 300$ K *and found the value* $K^0 = 11.3\times10^9$ mm^2/s^2 *(which we assumed to be given above) from PT criterion (53).*

The temperature distribution in the nucleus after PT is shown in Fig. 12. The homogeneous temperature increase due to the term $-\frac{\Delta s_0 \theta_0}{\nu}$ is equal to 111 K, i.e. this is the main contribution to temperature variation. Due to the higher yield stress in the nucleus and the presence of relatively high transformation shear as an inelastic (eigen) strain, the plastic strain in the nucleus for the given problem is small and much smaller than in shear bands near the nucleus. The heat source related to stress work is mostly due to transformation work. Stresses are quite heterogeneously distributed in the nucleus and change the sign. In the upper and lower corners of the nucleus the stress work is negative and the temperature is lower than 411 K, in other parts of the nucleus the stress work produces additional heating.

The effective temperature θ_{ef} found from PT criterion (53) is equal to 367 K. At isothermal approximation the PT starting temperature would be 367 K, i.e. allowing for adiabatic heating the transformation starting temperature decreases to 67 K. Allowance for an effective temperature of 367 K instead of $\theta_s = 300$ in kinetic Eq. (44) or (48) is equivalent to a decrease in activation energy by a factor of 1.223.

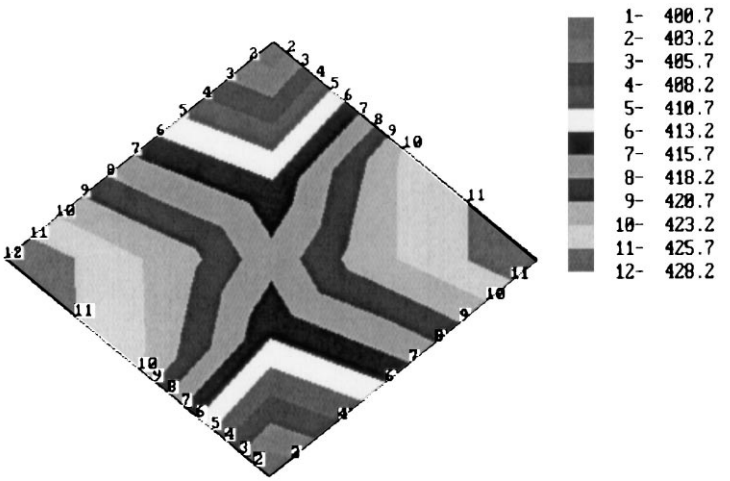

Fig. 12. Temperature distribution in nucleus 1 after PT ($\theta_s = 300$ K, $\theta_{e,f} = 367$ K).

4.3. Phase transition in a spherical particle within a cylindrical sample

Let us consider axisymmetric problems for a unit cell consisting of a spherical inclusion within a cylindrical matrix (Figs. 13 and 14). At stress controlled boundary conditions problems related to PT in spherical inclusion were solved by Levitas et al. (1998a) for coherent and incoherent interfaces and an interface with decohesion. Transformation of graphite particles embedded in an iron matrix (cast iron) into diamond is a possible example. The result was obtained that the smallest transformation work corresponds to a coherent interface. Incoherence at low friction and decohesion at the interface favors the PT condition significantly. The results obtained exhibited mutual assistance of various micromechanisms of inelasticity. The external stress in the examples considered was too low to initiate plasticity, sliding and decohesion without PT. PT without plasticity, sliding or decohesion at the interface could not occur either, because the driving force was too small. Consequently, each of these processes could not proceed separately. When at least two processes occur simultaneously, they help each other by the field of internal stresses and both are possible.

Based on our experience (Levitas et al., 1999), we expect solutions under prescribed forces and displacements to be qualitatively different. In addition, an important aspect related to the necessity to apply stability analysis and global PT criterion (41) to the description of competition between plasticity and PT arises for prescribed displacements. That is why we consider here displacement controlled boundary conditions.

Assume that under the applied external axial displacement increment and the given homogeneous temperature the spherical nucleus undergoes the dilatational transformation with $\varepsilon_{o2} = -0.005$. For reasons of symmetry, Fig. 13 shows a quarter of the unit cell of the composite, where X_1 is the horizontal axis of symmetry and

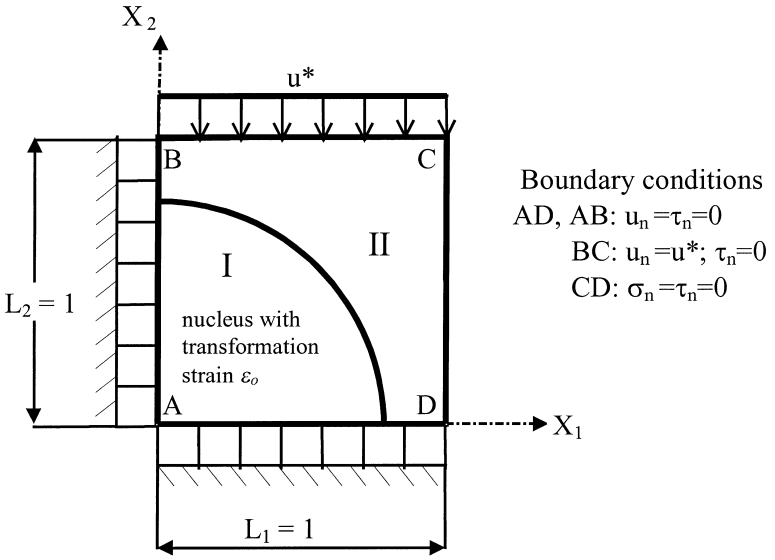

Fig. 13. A quarter of cross-section of the cylindrical matrix with a spherical nucleus.

X_2 is the axis of revolution, respectively. A coherent interface between the particle and the matrix is assumed. The yield stresses for the matrix and the inclusion are the same and equal to $\sigma_y = 200$ MPa before PT. After beginning the PT the nucleus is assumed to be elastic, which corresponds to infinite yield stress in transforming region. The volume fraction of the nucleus is $c = 0.28$. The following boundary conditions apply:

- along AB and AD boundaries $u_n = 0$, $\tau_n = 0$ (from the symmetry condition);
- along CD boundary $\sigma_n = \tau_n = 0$ (free surface);
- along BC boundary $u_n = u^*_{max}$, $\tau_n = 0$.

The PT is simulated by increasing the compressive transformation strain ε_o from 0 to -0.005. To obtain the value of the transformation work φ the elastoplastic problems are solved incrementally with a transformation strain increment $|\Delta\varepsilon_o| = 0.0005$.

Five different values of the maximum prescribed displacement u^*_{max} are considered, namely

$$u^*_{max} = 0.003;\ 0.004;\ 0.0045;\ 0.0065;\ 0.011. \tag{54}$$

As in the previous problem, the prescribed displacements grow proportionally to the order parameter ξ, see Eq. (50), and the transformation strain grows proportionally

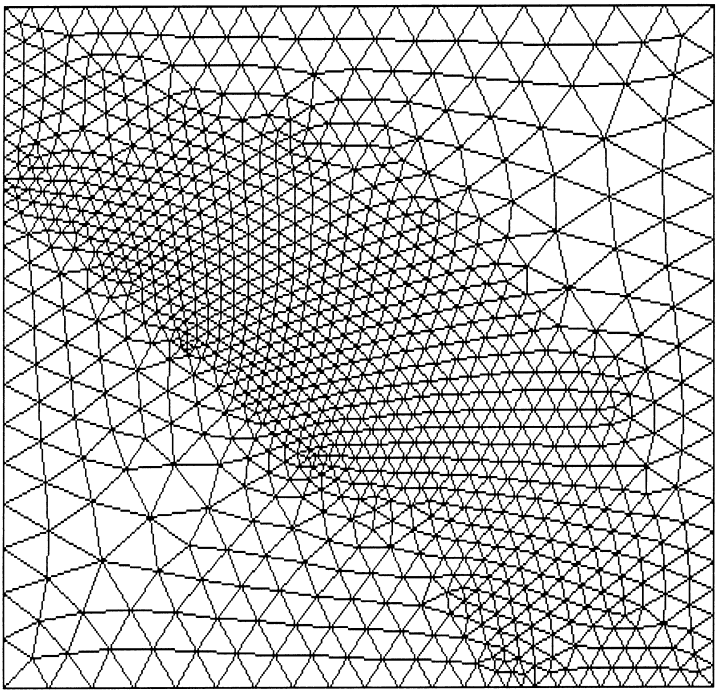

Fig. 14. Finite element mesh with refinement near the interface.

to the prescribed displacement. For all cases we start PT at the at the macroscopic strain $\varepsilon_1 = \frac{u_1^*}{L_2} = 0.001\%$ when the equivalent Mises stress in the matrix reaches the yield stress which corresponds to strain-induced rather than stress-induced PT. Here $L_2 = 1$ is the initial height of the sample. In Fig. 15 the calculated macroscopic stress P-vertical displacement u^* curves for the sample under consideration and corresponding values of the transformation work φ are presented.

The macroscopic axial stress P is obtained from the problem solution and averaging over the boundary CD. Curves 1–5 correspond to the PT in a spherical particle, curve 6 — for deformation without PT (perfectly plastic behavior). Two opposite factors related to PT are responsible for the shape of the stress-strain curve:

- appearance of additional transformational deformation modes, namely transformation strain in the particle and plastic strain in the matrix induced by transformation, i.e. transformation induced plasticity (TRIP);
- strengthening due to assumed infinite yield stress of the martensitic product.

For curves 3–5 additional transformational deformation modes exceed the prescribed strain, and thus macroscopic elastic strain and stress decreases during the

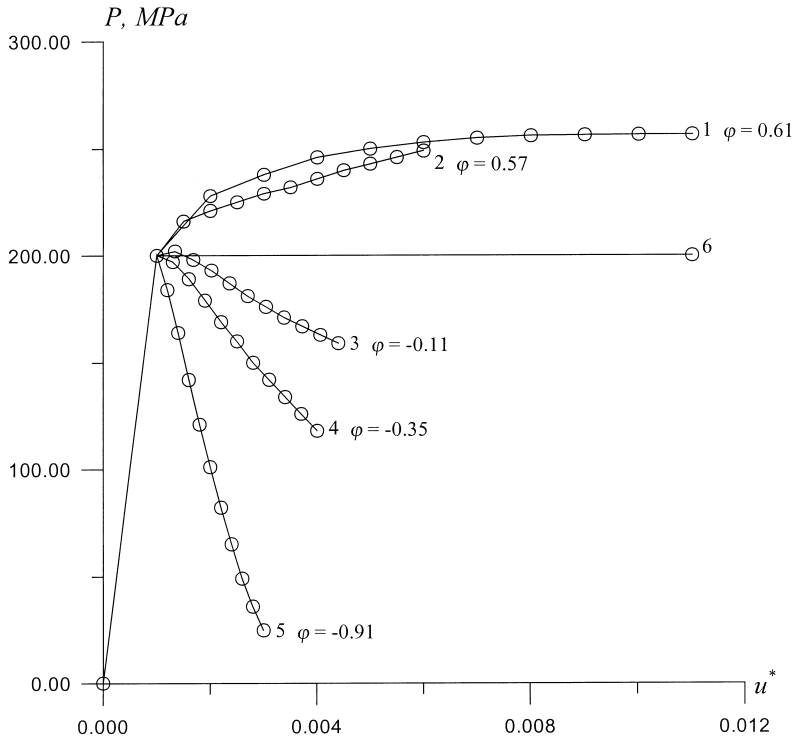

Fig. 15. Relationships between external averaged axial stress P and vertical displacement u^* (at different values u^* after finishing the PT).

transformation. The transformation work for these curves is negative, i. e. stresses resist the growing transformation strain. For curves 1 and 2 the prescribed strain exceeds the transformation strains and strengthening due to the infinite yield stress in the transforming region leads to higher stresses and positive transformation work.

As the transformation volumetric strain is five times smaller than in the previous problem, the transformation shear is zero and plastic strains are small, the temperature increase due to stress work is negligible in comparison with the term $\Delta\theta = -\frac{\Delta s_0 \theta_0}{v} = 111\,\mathrm{K}$ (the same properties as in the previous problem are used). Consequently, $\theta_{\mathrm{ef}} - \theta_{\mathrm{s}} = 55.5\,\mathrm{K}$.

If we know the PT starting temperature and K^0, then from the PT criterion (53) we can find the corresponding value of the transformation work φ and choose the prescribed displacement in Fig. 15 at which PT can occur. When the displacement is given, then the transformation work φ can be calculated and the PT temperature can be defined from the PT criterion (53).

As was mentioned in Section 2, the solution without PT (curve 6 in Fig. 15) is always possible, because it satisfies all the equations of continuum thermodynamics. To choose which solution — with PT or without PT — will be realized, we can use stability analysis. According to the stability criterion (41), when the $P - u^*$ curve for the solution with PT (curves 1 and 2 in Fig. 15) exceeds the $P - u^*$ curve for the solution without PT, the PT does not occur, despite the fact that the local PT criterion can be satisfied. In the opposite case (curves 3–5 in Fig. 15) the deformation process with PT is more stable. Such a situation can occur at high temperature when a large transformation work is required for PT. This suggests a possible criterion for the determination of the M_{d} temperature. The maximum temperature M_{d} at which PT can be caused by plastic straining is limited not by thermodynamics (because the higher transformation work can be obtained, see curves 1 and 2 in Fig. 15), but by the impossibility of PT from the viewpoint of stability analysis.

4.4. Appearance of martensitic plate in elastoplastic material

Let us consider the appearance of a small temperature-induced martensitic plate in elastoplastic material for the case of a plane strain state, Fig. 16. To evaluate the condition of martensitic plate formation, calculations were made for five cases of the appearance of the nucleus in regions I; I-II; I-III, I-IV; I-V, respectively, i.e. with different ratios of its width and length. The following elastoplastic properties of steel were used in calculations:

yield stress $\sigma_{\mathrm{y}} = 250$ MPa for an austenitic matrix and $\sigma_{\mathrm{y}} = 800$ MPa for a martensitic nucleus. The boundary of the sample is free from stresses, which is in line with experiments for temperature-induced PT. For our calculations the transformation deformation gradient $\mathbf{F}_{\mathrm{t}}$ is subdivided into 60 increments. The final value of $\mathbf{F}_{\mathrm{t}}$ has the following components in the cartesian coordinate system $X_1\,X_2\,X_3$

$$(F_{\mathrm{t}})_{11} = (F_{\mathrm{t}})_{33} = 1,\ (F_{\mathrm{t}})_{12} = 0.2,\ (F_{\mathrm{t}})_{22} = 1.026, \tag{55}$$

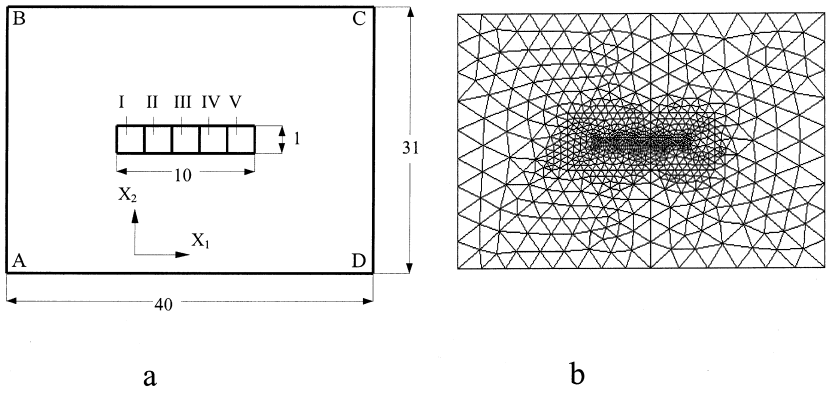

Fig. 16. Cross-section (a) with stress free boundary and FE mesh (b) of a sample with a nucleus (regions I–V).

the other components are zero. The stresses and the value of the transformation work φ was determined by solving the elastoplastic problem with incrementally enlarged transformation deformation gradient.

According to the numerical results the martensitic plate deforms practically elastically with the exception of small regions near short sides. In the parent phase the plastic strains are concentrated around the transformed plate. The distributions of the accumulated plastic strain are presented in a paper by Idesman et al. (1999b). The relation between the transformation work and ratio of width to length of nucleus $x = \frac{l}{h}$ is obtained and approximated by the parabolic function

$$\varphi = \bar{A} + Bx + Cx^2, \quad \bar{A} = -72.11\,\text{MPa},$$
$$B = 6.40\,\text{MPa}, \quad C = -0.29\,\text{MPa}. \tag{56}$$

It is clear that assumptions related to the plane strain state and the infinite nucleus in the X_3 direction used here and below for problems on PT and fracture are unrealistic from a kinetic point of view and the principle of the minimum of transforming mass. A small three dimensional nucleus will appear for such problems with the higher transformation rate; however, solutions of three-dimensional problems are much more time consuming. So to meet the ends in a simplified way, we will assume that we know and will not vary the actual thickness of the nucleus b in the X_3 direction and will use the plane strain solution for the determination of X and to allow for the surface energy.

The principle of the minimum of transformation time Eq. (45) results in

$$\left(A_1 + Bx + Cx^2\right)lh - 2\Gamma(l + h) \;\rightarrow\; \max_{x,l}, \tag{57}$$

where $A_1 := \bar{A} - K^0 - \rho\Delta\psi_\theta - E_a$, Γ is the surface energy. Application of the principle Eq. (57) leads to two algebraic equations

$$A_1 + 2Bx + 3Cx^2 = \frac{2\Gamma}{h};\ A_1 x - Cx^3 = \frac{2\Gamma}{h} \tag{58}$$

which are equivalent to a cubic equation with respect to x. Analysis shows that this equation has a thermodynamically admissible solution for a very high driving force and small activation energy only. Applying the principle of the minimum of transforming mass Eq. (47) together with the thermodynamic criterion Eq. (46)

$$\left(A + Bx + Cx^2\right)l = 2\Gamma(1+x);\ A := \bar{A} - K^0 - \rho\Delta\psi_\theta, \tag{59}$$

we obtain

$$\frac{V_n}{b} = lh = \frac{l^2}{x} = 4\Gamma^2 \frac{(1+x)^2}{x(A + Bx + Cx^2)^2} \rightarrow \min_x, \tag{60}$$

and the explicit expressions for ratio of width to length of a thermodynamically admissible nucleus and its length. In particular, at $x \gg 1$ we get

$$x = -\frac{B + \sqrt{B^2 + 12AC}}{6C},\ l = \frac{2\Gamma(1+x)}{(A + Bx + Cx^2)}. \tag{61}$$

The higher the driving force, the smaller the nucleus and the smaller the transformation time. For example, at $A = 0$ we get $x = 7.36$, $l = 0.533\Gamma$ and at $A = -30$ we obtain $x = 10.61$, $l = 4.40\Gamma$.

Substituting $V_n = lhb$ in the kinetic equation, Eq. (48), we determine the transformation time. If the width of the nucleus obtained with the help of Eq. (61) is smaller than the interatomic distance a in the X_2 direction, then we put $l = a$ and determine the thermodynamically admissible x from Eq. (59). The transformation time is determined by Eq. (44) at $V_n = lab$.

Consequently, the following typical cases in the determination of the width and length of plate are found: solely from the principle of the minimum of transformation time and the kinetic equation without any constraints; from the principle of the minimum of transformation mass and the thermodynamic criterion of SC; as an interatomic distance and from the thermodynamic criterion.

4.5. Growth of martensitic plate inside the austenitic matrix

One problem presented here differs from the previous one by the sizes of the regions I–V, Fig. 17. First we consider PT in the region I. The stress and strain fields after the appearance of martensitic plate with the aspect ratio $x = 4$ (the region I) are used as initial data for the study of the plate growth. Then we model the plate

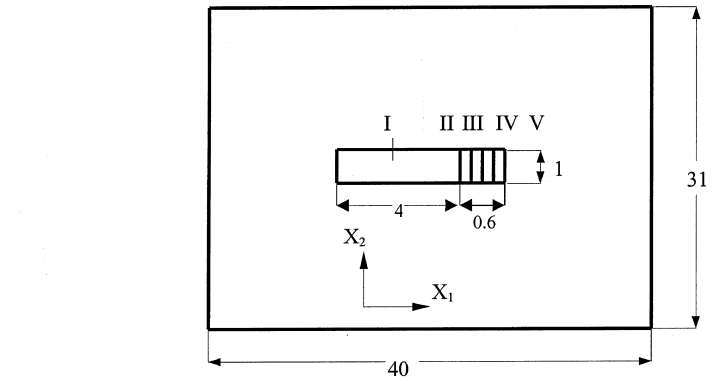

a

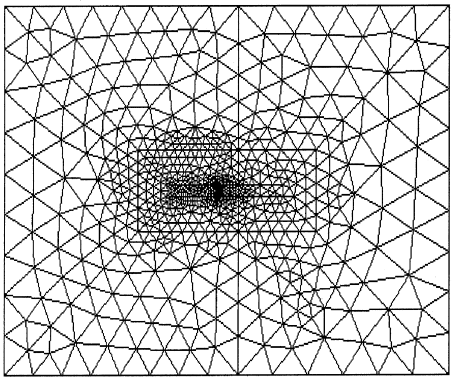

b

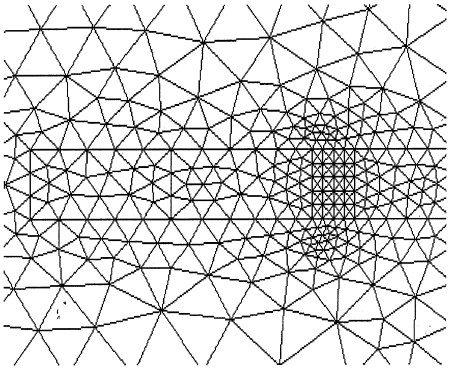

c

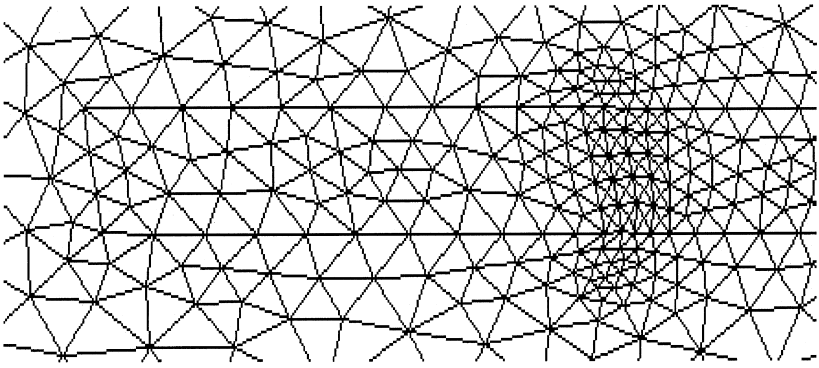

d

Fig. 17. Cross-section of a sample with subsequently transforming regions I–V (a) and FE mesh before (b — for a whole sample, c — near transforming regions) and after (d — near transformations regions) transformation.

growth by subsequent PT in regions II–V, i.e. first in region II, then in region III and so on.

A refined finite element mesh within and near the transforming zone is used. Each transforming region during the plate growth (II, III, IV and V) contains 20 finite elements. The space step for interface motion (width of region II, III and so on) is chosen to be 0.15 of the plate width.

It is convenient to introduce the process parameter ζ as follows: $\zeta = \sum_{i=1}^{k} \xi_i$, where k designates the number of the transforming region in Fig. 17 and ξ_i is the order parameter ξ in region number i. For example, when $k = 1$, PT occurs in the large plate I and $\zeta = \xi_1$. After finishing the PT in the plate and starting the transformation in region II, we have $k = 2, \xi_1 = 1$ and $\zeta = 1 + \xi_2$. When PT is completed in region II and starts in region III, then $k = 3, \xi_1 = \xi_2 = 1$ and $\zeta = 2 + \xi_3$ and so on.

The deformed mesh in the transformed region (Fig. 17d) together with isobands of accumulated plastic strain (Figs. 18 and 19) present very complex and heterogeneous strain (and consequently stress) fields in austenite and martensite and their non-monotonous variation with the growth of the process parameter ζ. Positive values of shear stress and plastic shear strain correspond to the direction opposite to transformation shear.

The transformation work decreases significantly from the value -50.3 MPa for the appearance of the large plate I to -100.8 MPa for region V with a saturation which is expected for the steady stage of plate growth (Fig. 20). Such a decrease is caused by interaction between transformation strain in the currently transforming region, transformation strain in the previously formed plate, the plastic strain field due to the previous transformation process and due to currently growing transformation strain as well as by the three times higher yield stress of martensite.

It is clear that if the driving force in the nucleation of a martensitic plate is smaller than the value calculated for a steady growth state, the plate growth will be arrested.

In Figs. 21 and 22 the variation of the shear stress $\bar{\tau} := \frac{1}{V_n}\int_{V_n} \tau \mathrm{d}V_n$ and the variation of the plastic shear strain $\bar{\gamma} := \frac{1}{V_n}\int_{V_n} \gamma \mathrm{d}V_n$, averaged over each region I–V during the sequential PT in regions I–V, are presented.

During the transformation in the large plate I, the averaged plastic shear strain (Fig. 22) is very small. The averaged shear stress which resists the transformation strain grows very intensively (linearly) in an elastic regime and it is practically constant in a plastic regime (Fig. 21). It decreases slightly after finishing the PT in region I and at each next transformation event.

It was expected that the shear stress and plastic strain averaged over the region contacting the currently transforming region have the same sign as the transformation strain. It appears, however, that due to very strong stress heterogeneity this is not the case. During the PT in plate I the shear stress and plastic strain averaged over region II are positive. The same situation takes place for all the other transforming regions.

Due to the large field gradients near the transforming region, the shear stress averaged over the regions, which are not in contact with the currently transforming region, has the same sign as the transformation strain. For example, during the transformation in plate I the shear stress averaged over regions III, IV and V is

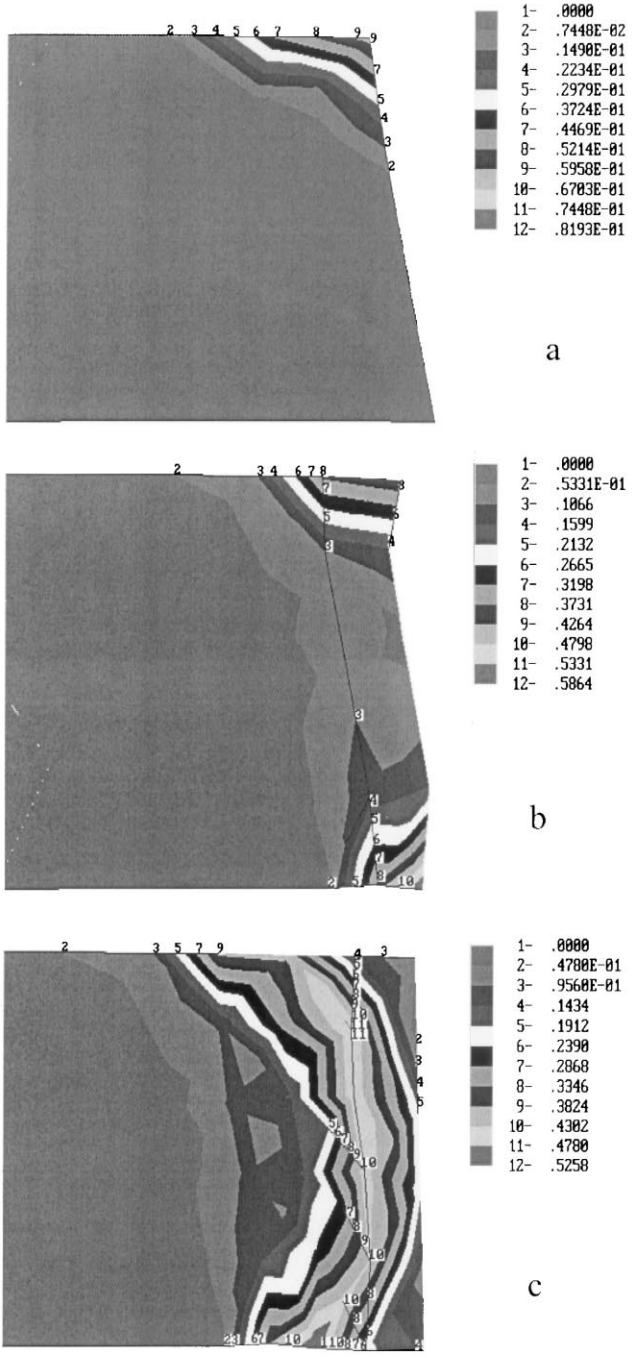

Fig. 18. Isobands of the accumulated plastic strains in the right part of the martensitic plate after transformation in regions I (a), I–III (b), I–V (c).

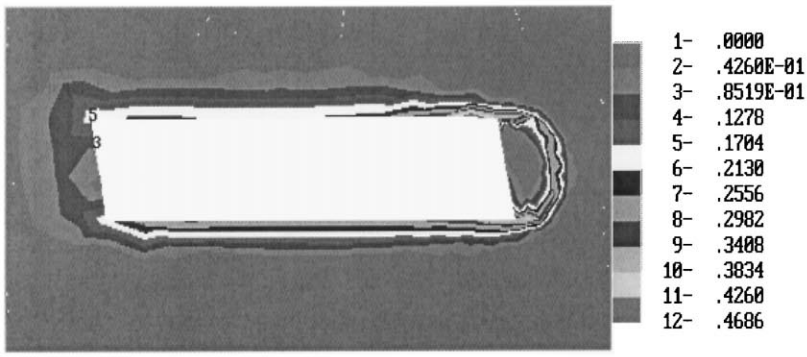

a

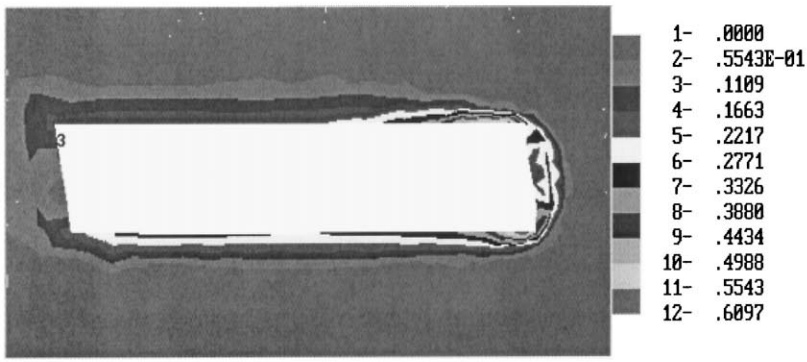

b

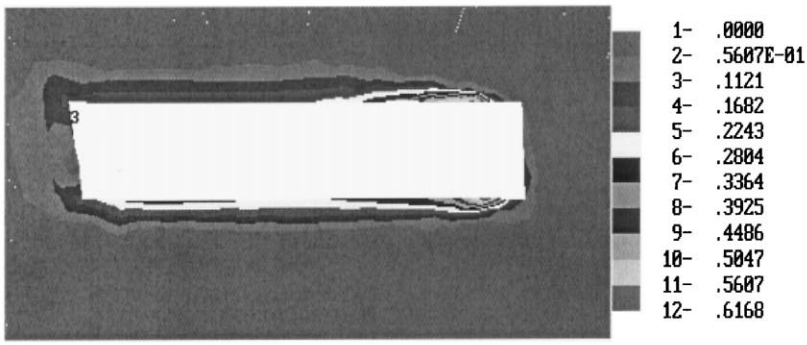

c

Fig. 19. Isobands of the accumulated plastic strains near transformation regions after transformation in regions I (a), I–III (b), I–V (c).

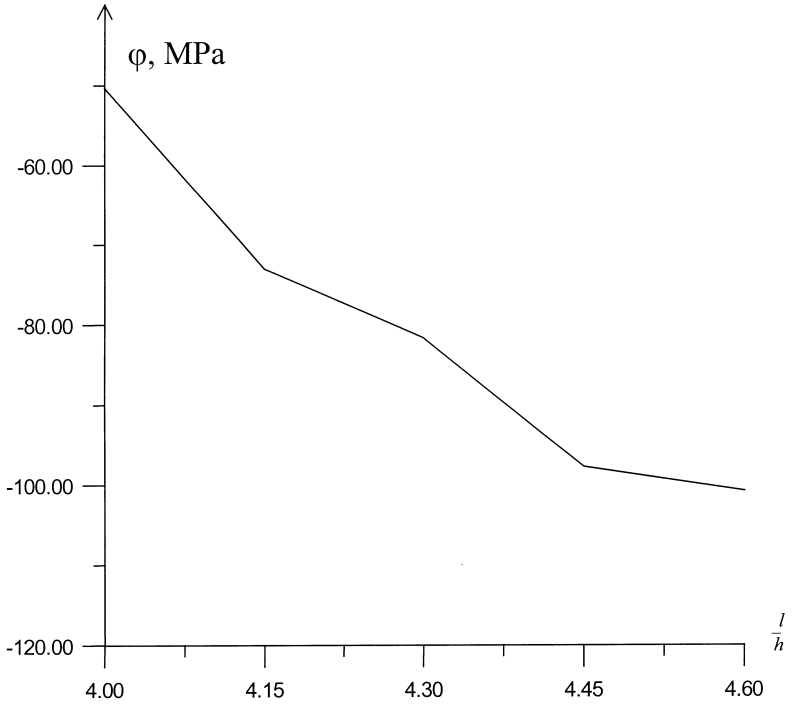

Fig. 20. Transformation work φ as a function of ratio l/h.

negative. In region III, due to large gradients, the situation is very surprising, because the shear stress and plastic strain averaged over this region have different signs. The averaged shear plastic stress in regions IV and V has the same negative sign as the averaged shear stress.

In the transformation in region II, the shear stress averaged over region II (which resists the transformation) grows significantly due to the jump-like change in the yield stress. This is the reason for the decrease in transformation work in comparison with the transformation work for plate I. At some stage in the transformation, the stress is high enough to cause the plastic straining in martensite in addition to plastic strain inherited by martensite from austenite.

With respect to the transformation in region III the averaged shear stress and plastic strain behave in a similar way to those with respect to the transformation in the region II; the same is qualitatively true for all the other transforming regions.

An interesting cyclic change of averaged plastic shear occurs in regions IV and V, respectively. In the transformation in plate I, the sign of these plastic shears coincides with the sign of the transformation strain. Then, after some stage of elastic straining, plastic shears grow in the opposite direction.

The deformed mesh in the transformed region (Fig. 17) together with isobands of accumulated plastic strain (Figs. 18 and 19) allow deeper inside into non-homogeneous distributions of shear strains in addition to the information given in

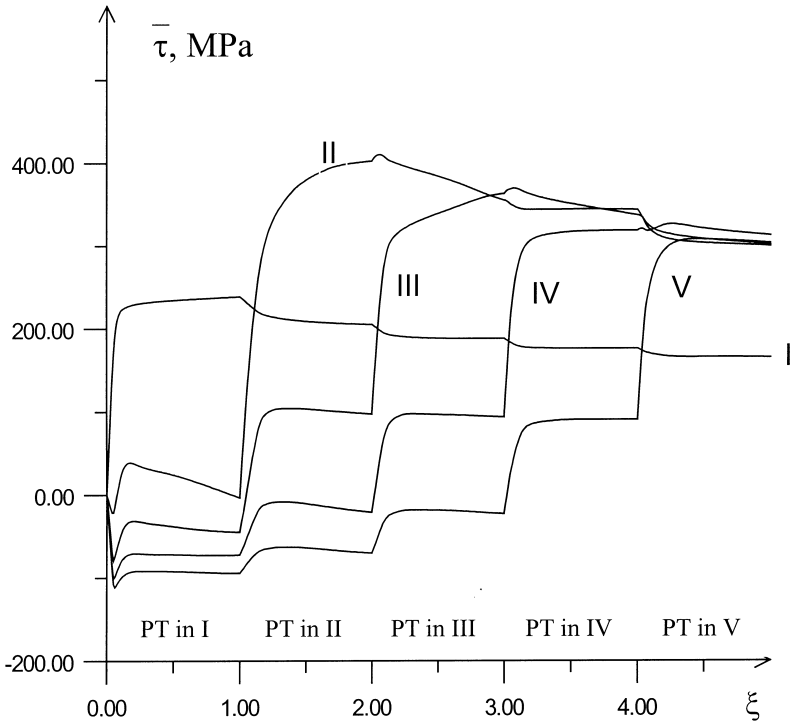

Fig. 21. Variation of shear stress $\bar{\tau}$ averaged over each region I, II, III, IV, V (designated near the curves) during sequential phase transformation in regions I, II, III, IV, V.

Fig. 22. It seems at first glance that the results in Fig. 22 are contradictory. For example, the plastic shear is almost equal to the transformation shear with the opposite sign in region III, i.e. region III has to be nearly undeformed overall. This is not the case, and Figs. 17–19 allow us to explain this seeming contradiction by the very heterogeneous deformation in this region.

After PT in plate I there is a small region near the short side of the plate in which plastic strain is very small (Fig. 19a). Plastic strain is also very small near the martensitic plate after completing the PT in region V (Fig. 19c), which is in agreement with experiments. This is related to the relatively small shape of the contour of the martensitic plate (see the deformed mesh in Fig. 17). Such a final picture, if observed experimentally, can give the impression that austenite deforms (excluding the narrow zone) elastically and martensite plastically. As follows from considering the transformation process, intense plastic deformations near the interface from the austenite side are inherited by growing martensite and make a very important contribution to stress variation and the driving force in the transforming region.

The wave-like profile of the martensitic plate after PT in region III (Fig. 18b) is also very surprising: the resulting shear near the corners is directed in the opposite direction to the transformation shear and is significant.

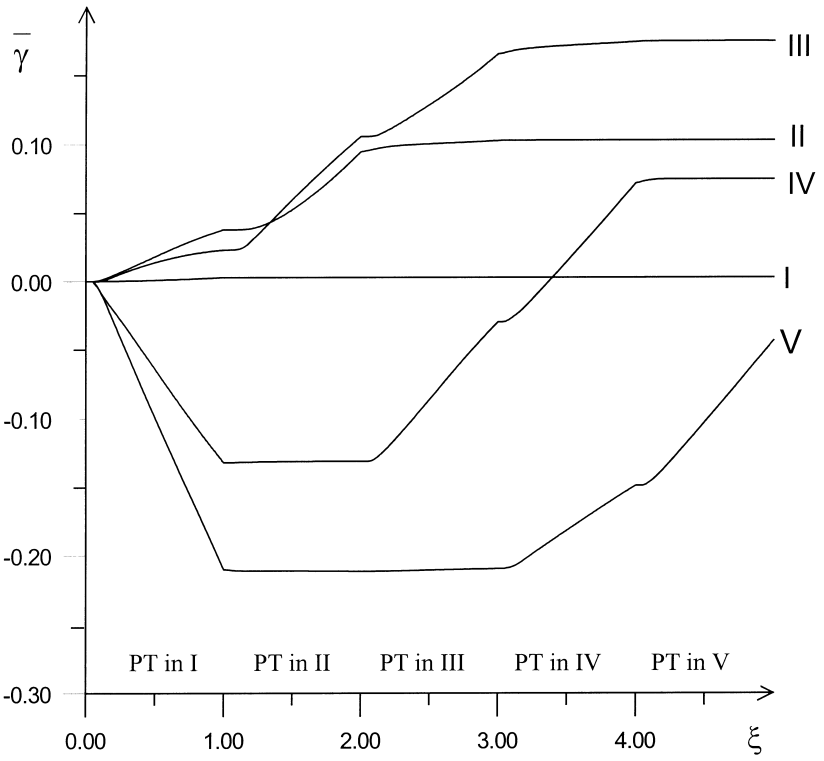

Fig. 22. Variation of plastic shear strain $\bar{\gamma}$ averaged over each region I, II, III, IV, V (designated near the curves) during sequential phase transformation in regions I, II, III, IV, V.

As follows from Fig. 21, the resisting shear stress in region II during the PT is much higher than in regions IV and V, i.e. the transformation shear work in region II is smaller than in regions IV and V. At the same time the total transformation work in region II is higher than in regions IV and V (Fig. 20). This emphasizes the importance of the work of normal stresses along transformation dilatation, which is only responsible for such a difference.

To summarize, very nontrivial and heterogeneous stress-strain fields in austenite and martensite and their nonmonotonous variation during the transformation process are found. The plastic shear strain in some points can reach 60% in the direction of transformation shear and, after some elastic stage, change sign and vary by 40%. The profile of the moving interface (short side of a plate) varies in a nontrivial way as well (Fig. 18): after the expected transformation shear the wave-like profile with the total shear near the corners directed in the opposite direction to transformation shear follows, and finally a practically undeformed vertical line (as before transformation) is formed. These results demonstrate the necessity of finite strain treatment. The results obtained support the idea that plastic accommodation can lead to growth arrest and to the technologically important plate/lath morphological

transition (Olson and Cohen, 1986; Haezebrouck, 1987). More detailed analysis of the interface propagation though elastoplastic material will be given in a paper by Levitas et al. (2000).

4.6. Appearance of a single twin in elastoplastic material

Continuum mechanical approach to interaction between slip and twinning was considered in papers by Staroselsky and Anand (1998), Schlogl and Fischer (1997) and references there in. Continuum thermodynamic twinning criterion at finite strains was suggested by Levitas (1998a). The first example of a numerical implementation of this criterion to the appearance of a single twin in elastoplastic material at finite strains caused by external shear stresses was reported in a paper by Idesman et al. (1999b). In particular, the influence of plastic properties on twin formation was considered. Here the effect of the variation of external shear stress as well as the prescribed displacement on twinning is investigated.

We take the same cross-section of a sample as for the problem in Section 4.4, i.e. a twin forms a single plate in the parent phase. The differences to the problem in Section 4.4 are:

(a) the transformation deformation gradient has only a large shear component

$$(F_{t2})_{11} = 1,\ (F_{t2})_{12} = 0.707,\ (F_{t2})_{21} = 0,\ (F_{t2})_{22} = 1,\ (F_{t2})_{33} = 1, \tag{62}$$

the other components are zero,

(b) the plastic properties of the two phases are the same, and the yield stress is $\sigma_y = 600$ Mpa.

Due to the very high transformation shear a finite strain formulation is of great importance. We consider twin formation due to external shear stresses which are constant during the twinning. The following boundary conditions apply (Fig. 16):

- along BC boundary $u_n = 0$, $\tau_n = \tau^*$;
- along AD boundary $u_n = u_\tau = 0$;
- along AB and CD boundaries $\sigma_n = \tau_n = 0$ (free surface).

The value of the external shear stress τ^* varies in the range [180÷270 MPa]. The sequence of calculations is the same as for the problem with martensitic PT. To solve the elastoplastic problem the transformation deformation gradient $\mathbf{F}_{t2}$ and the order parameter ξ are subdivided into 300 increments.

The calculated values of transformation work φ with the various applied external shear stresses are presented in Fig. 23; the twin aspect ratio $x = 10$. It is interesting that for the nonlinear problem considered here the diagram in Fig. 23 is practically linear. At $\tau^* < 250$ MPa twinning is impossible at any $K^0 \geqslant 0$ because the transformation work $\varphi < 0$. At $\tau^* > 250$ MPa the possibility of twinning depends on the value of K^0.

Solving the problem for different aspect ratios of the single twin and approximating analytically the values of φ we can repeat the procedure described in Section 4.4

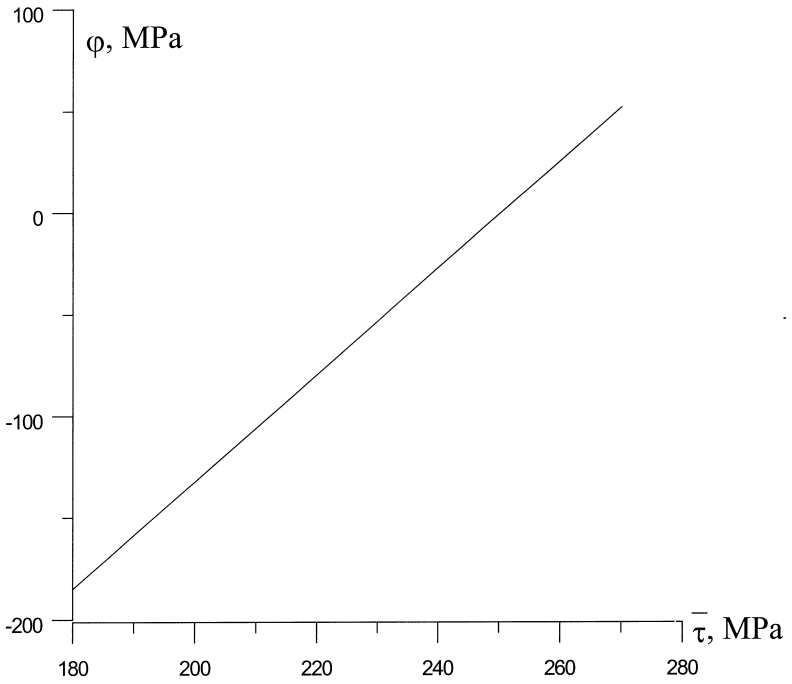

Fig. 23. Transformation work φ as a function of the external shear stress $\bar{\tau}$.

for the determination of the actual geometrical parameters of the twin for prescribed τ^* and material properties.

The problem of the appearance of a single twin was also solved for an applied external horizontal displacement at the surface BC (instead of the external shear stress τ^*) which grew simultaneously with transformation deformation gradient in the twin (as for the problems in Sections 4.2, 4.3). In particular, subsequent twinning the region I, then II,... and V (see Fig. 16) was considered. It appears that the transformation work φ is practically the same for each transforming region, i.e. it is constant during such a growth process. A similar analysis of the choice of a stable solution, as was done for the problems in Sections 4.2, 4.3, can be applied to twinning as well.

5. Fracture in elastoplastic materials

There is a considerable literature on the finite element study of fracture in elastoplastic materials based on the consideration of crack propagation, see for example the book by Atluri (1997) and references there in. Some drawbacks of the consideration of fracture in elastoplastic materials as a crack propagation are related to the lack of noncontradictory thermodynamic criteria and are analyzed by Levitas (1998b, 2000a,b). In the same papers it was suggested that one could consider fracture as a

special deformation process in some finite volume which is defined as a part of a solution to the boundary-value problem from extremum principle suggested. The thermodynamic fracture criterion and the thermodynamically consistent kinetic equation is derived. Model problems on void nucleation and Dugdale-type crack propagation in elastoplastic material are solved analytically.

In the present paper first numerical solutions based on the same approach as that described in Section 2 are presented. Some preliminary results can be found in a short communication by Levitas and Idesman (1998).

Let us consider a model problem of fracture in a sample with initial edge notch under tensile stress and plane strain state. The case of small elastic, but large plastic strains is assumed. For numerical simulation of fracture the 'inverse' problem is considered, i.e. the position and size of the fracture region (nucleus) are prescribed in advance, and then the condition for fracture is defined from the fracture criterion. Such an approach includes a finite element solution of the elastoplastic problem with the decreasing elastic and plastic properties in the fracture region during fracture.

The cross section of a sample and the finite element mesh are given in Fig. 24. We consider isotropic elastic-perfectly-plastic material with the yield stress $\sigma_y = 800$ MPa. The following boundary conditions are applied:

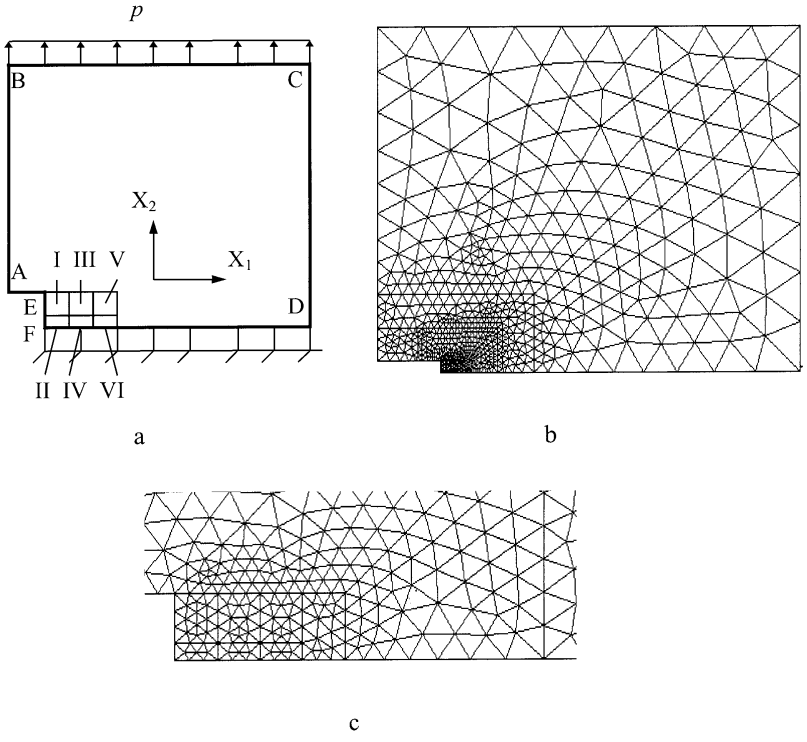

Fig. 24. The cross-section of a sample (a), finite element mesh (b) and finite element mesh near edge notch (c).

- along FD, boundary $u_n = 0, \tau_n = 0$ (the symmetry plane);
- along BC boundary $\sigma_n = p = 700\,\text{MPa}, \tau = 0$ (p is the prescribed normal stress);
- along AB, CD and AEF boundaries $\sigma_n = 0, \tau_n = 0$ (free surface).

The following presumptions hold:

(a) for simplicity the fracture region is assumed to be rectangular, and various possible values of its length and height as well as its positions are studied;
(b) in the fracture region the Poisson's ratio during fracture is constant; Young's modulus and yield stress during fracture are homogeneously changed for 40 steps from initial values of undamaged material to zero and their ratio is constant during the property variation.

For isotropic Hooke's law

$$\varphi = \varphi^d + \varphi^v, \varphi^d := -\frac{1+\nu_o}{3V_n}\int_{V_n}\int_{E_1}^{0}\frac{\sigma_i^2}{E^2}\mathrm{d}E\mathrm{d}V,$$
$$\varphi^v := -\frac{3(1-2\nu_o)}{2V_n}\int_{V_n}\int_{E_1}^{0}\frac{\sigma_o^2}{E^2}\mathrm{d}E\mathrm{d}V, \tag{63}$$

where σ_o is the mean stress, σ_i is the stress intensity, ν_o is Poisson's ratio.

The distribution of equivalent stress before fracture is shown in Fig. 24a. The following cases of a possible fracture region are studied: fracture occurs

(a) in regions I, II;
(b) in regions I–IV;
(c) in regions I–VI;
(d) in region II;
(e) in regions II, IV;
(f) in regions II, IV, VI.

Additionally the following possible scenarios of fracture progress are considered:

(g) fracture occurs first in regions I, II; then in regions III,IV; finally in regions IV,VI; and
(h) fracture occurs first in region II; then in region IV; finally in region VI;
(i) void nucleation ahead of the crack tip occurs in region VI or IV;
(j) fracture in region II or IV after void nucleation in region VI.

The ratio between the heights of regions I and II is 3; the lengths of regions I, III, V are the same. The results of the calculations are presented in Figs. 25–27 and in Table 1 where zones I–VI are schematically shown. The distribution of equivalent stress after fracture in regions I–VI is shown in Fig. 25b. The equivalent stress reaches the yield stress almost in the entire band between the fracture region and the

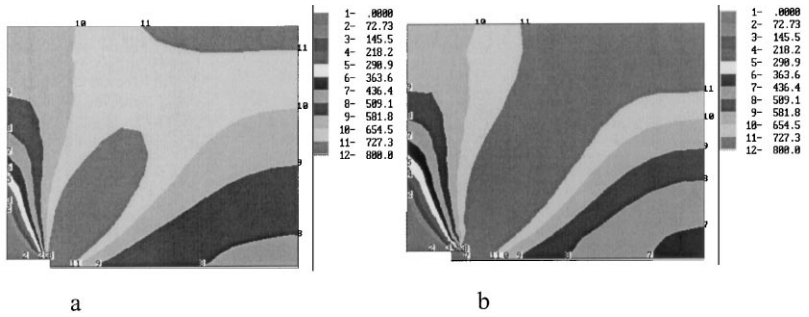

Fig. 25. Distribution of equivalent stress before fracture (a) and after simultaneous fracture in regions I–VI.

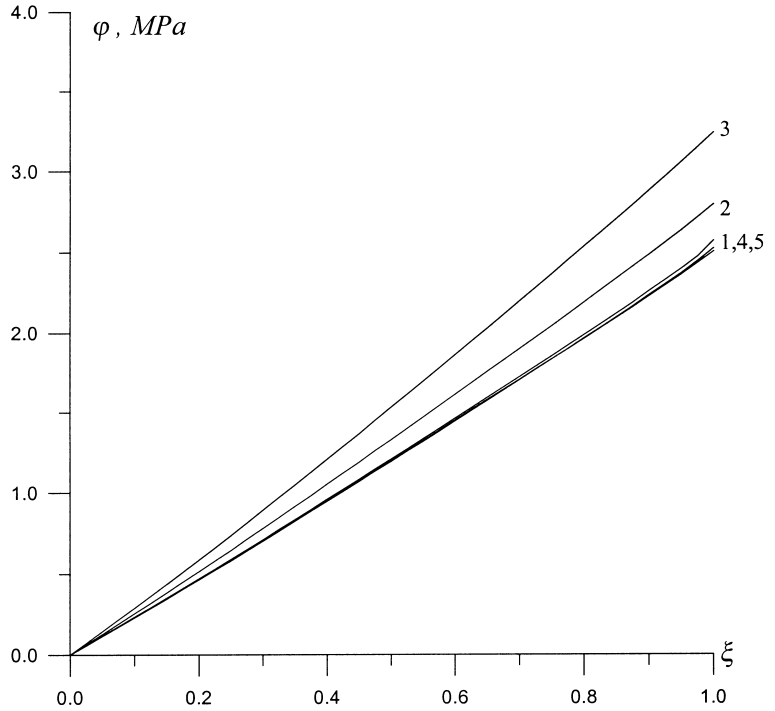

Fig. 26. Driving force φ as function of ξ. Fracture occurs: 1 — in regions I, II [$\varphi(\xi = 1) = 2.5$ Mpa]; 2 — in regions I–IV [$\varphi(\xi = 1) = 2.79$ Mpa]; 3 — in regions I–VI [$\varphi(\xi = 1) = 3.24$ MPa]; 4 — in regions III, IV after fracture in regions I, II [$\varphi(\xi = 1) = 2.52$ MPa]; 5 — in regions V, VI after fracture in regions I, II and III, IV [$\varphi(\xi = 1) = 2.57$ MPa].

upper right corner of a sample. The attempt to increase the length (more than the length of regions I–VI) of the fracture region leads to divergence of the iteration algorithm; that means the impossibility of equilibrium due to a limit plastic state. The curves in Figs. 26 and 27 show the variation of the mechanical driving force φ

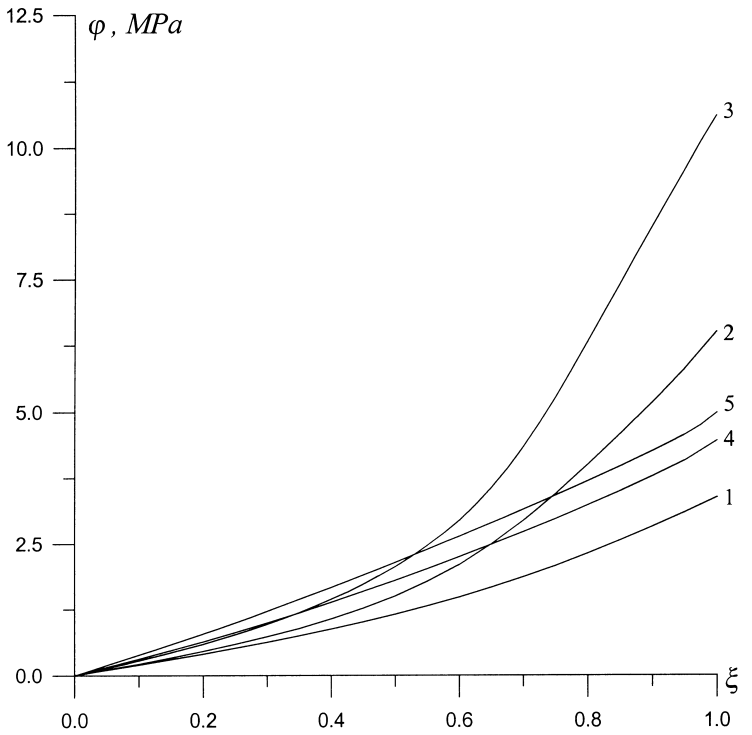

Fig. 27. Driving force φ as function of ξ. Fracture occurs: 1 — in region II [$\varphi(\xi = 1) = 3.38$ MPa]; 2 — in region II, IV [$\varphi(\xi = 1) = 6.48$ MPa]; 3 — in regions II, IV, VI [$\varphi(\xi = 1) = 10.59$ MPa]; 4 — in region IV after fracture in region II [$\varphi(\xi = 1) = 4.45$ MPa]; 5 — in region VI after fracture in regions II and IV [$\varphi(\xi = 1) = 4.97$ MPa].

during the fracture process. The driving force φ grows with the increase in a length of the fracture region, and the increase is sharper for a small height of the fracture region (Figs. 26 and 27). The decrease in height of the fracture region leads to an increase in the driving force φ (Fig. 26, 27).

The successive progress of the fracture region with a constant height yields practically the same value of the driving force φ in case (g), Fig. 26, which corresponds to stationary growth of the fracture region. A small increase in the driving force φ is obtained in case (h) for the successive fracture regions, Fig. 27, i.e. accelerated growth of the fracture region occurs.

For fracture in thin regions II, IV and VI the driving force is higher and growth is more intensive during the fracture propagation than for thick regions I, III and V (Table 1). However, the surface energy resists fracture stronger for a thin layer than for a thick layer. If fracture occurs simultaneously in regions II + IV or II + IV + VI rather than first in a small region II and then propagates through regions IV and VI, the driving force is higher, i.e. it is a more favorable scenario from the thermodynamic point of view. However, the transforming volume increases by factors 2

and 3, respectively. As a consequence, the kinetically subsequent growth is more favorable, provided that the thermodynamic criterion is satisfied.

We have also solved the problem presented in Fig. 24 for another value of the yield stress ($\sigma_y = 1 \times 10^3$ MPa) and obtained the results that the driving force φ is proportional to σ_y^2.

It is necessary to note that the part of the driving force φ^d due to variation of a deviatoric stress tensor in the fracture region is practically constant for all the cases considered and equals $\varphi^d = \sigma_y^2(1 + \nu_o)/3E_1$. It means that almost all the material points in the fracture region deform plastically.

At a relatively small surface energy a void nucleation in region VI will occur rather than crack (notch) growth. The mechanical driving force is much higher than for any scenario of crack propagation and pore nucleation in region IV (see Table 1). After void nucleation fracture propagates in the direction from void to notch. It is known that the void nucleation ahead of the crack tip is an actual physical mechanism of ductile fracture, however, we derived this rather than assuming it.

Let us introduce an analytical approximation of the numerical results obtained for fracture and analyze them.

(a) Let us consider fracture in a rectangular region with a dimensionless length L and height H which are equal to the actual length and height divided by the height EF of the notch (see Fig. 24a). We use the following simple relation between the driving force X, the length L and the height H

Table 1
Driving force φ for different scenarios of fracture

	φ, MPa	V_n	
Fracture in I, II	2.5	4	
Fracture in III, IV after fracture in I, II	2.52	4	
Fracture in V, VI after fracture in I — IV	2.57	4	
Fracture in II	3.38	1	
Fracture in IV after fracture in II	4.45	1	
Fracture in VI after fracture in II, IV	4.97	1	
Fracture in I — IV	2.79	8	
Fracture in I — VI	3.24	12	
Fracture in II, IV	6.48	2	
Fracture in II, IV, VI	10.59	3	
Fracture in VI	23.29	1	
Fracture in IV	10.62	1	
Fracture in II after fracture in VI	3.69	1	
Fracture in IV after fracture in VI	7.22	1	

 Initial;  Current.

$$\rho X = c_1 + c_2 L + + c_3 H + c_4 LH, \tag{64}$$

where $c_1 = -1.01$ MPa, $c_2 = 1.95$ MPa, $c_3 = 3.14$ MPa, and $c_4 = -1.8$ MPa are coefficients which approximate the data from Table 1. Then the thermodynamic fracture criterion (43), extremum principle (45) and constraint $(44)_2$ have the following form

$$y_1 = c_1 + c_2 L + c_3 H + c_4 LH - \frac{\Gamma}{H} \geqslant 0, \tag{65}$$

$$y_2 = (c_1 + c_2 L + c_3 H + c_4 LH - E_a) 2HL - \Gamma 2L \ \rightarrow \ \max_{L,H}, \tag{66}$$

$$c_1 + c_2 L + c_3 H + c_4 LH - E_a < 0, \tag{67}$$

$$a \leqslant L \leqslant L_{max}, \quad b \leqslant H \leqslant H_{max}. \tag{68}$$

Here a, b and L_{max}, H_{max} are the interatomic distances and the maximum distances from the notch tip to the boundary of the sample along axes X_1 and X_2, respectively, E_a is the activation energy. For simplicity we assume $K^0 = \Delta\psi_\theta = 0$ (these constants can be included in c_1). Such, we should find L and H which maximize a function y_2 [Eq. (66)] at constraints Eqs. (65), (67), (68). This problem is complicated and can be solved numerically. The more simple specific cases $H = \text{const}$, or $L = \text{const}$ (in particular $H = b$ or $L = a$) are analyzed below.

(b) First, the case of fracture in a rectangular region with a constant height H and a variable length L is considered. Then the Eq. (64) can be presented in the form

$$\rho X = C_1 + C_2 L, \tag{69}$$

with $C_1 = c_1 + c_3 H$ and $C_2 = c_2 + c_4 H$. Below we consider the case when $C_2 > 0$. The case $C_2 < 0$ can be analyzed in a similar way. The thermodynamic fracture criterion (43), extremum principle (45) and constraint $(44)_2$ are reduced to the following form

$$y_1 = C_1 + C_2 L - \frac{\Gamma}{H} \geqslant 0, \tag{70}$$

$$y_2 = (C_1 + C_2 L - E_a) 2HL - \Gamma 2L \ \rightarrow \ \max_{L}, \tag{71}$$

$$y_2 = (C_1 + C_2 L - E_a) 2HL - \Gamma 2L < 0. \tag{72}$$

An additional constraint

$$a \leqslant L \leqslant L_{max} \tag{73}$$

defines minimum and maximum admissible values of L. Consequently, we should find L which gives a maximum value of a function y_2 [Eq. (71)] at constraints Eqs. (70), (72), (73). From the condition $\frac{\partial y_2}{\partial L} = 0$ we obtain

$$L^{\diamond} = \frac{E_a + \Gamma/H - C_1}{2C_2}. \tag{74}$$

Check of a sign of the second derivative (H is a constant parameter)

$$\frac{\partial^2 y_2}{\partial^2 L} = 4C_2 H > 0 \tag{75}$$

leads to conclusion that at $L = L^{\diamond}$ the function y_2 has a minimum rather than maximum. Then a maximum value of y_2 is reached at the boundary of a region of variation of L, determined by the constraints. Let us consider a large value of E_a at which $L^{\diamond} \geqslant L_{\max}$ and the inequality (72) is met for L within a range defined by Eq. (73). At such a value of E_a a maximum of y_2 is reached at a minimum admissible value of L, determined from the thermodynamic constraints (70), i.e.

$$L = \frac{\Gamma H - C_1}{C_2}, \tag{76}$$

if this $L_o \geqslant a$; otherwise $L = a$. For smaller E_a, for which $L^{\diamond} < L_{\max}$, we have to check the value $L_{\max}$ as the possible solution of the extremum problem (71). Physically this means simultaneous separation of the sample along the axis X_1.

(c) Now let us consider fracture in a rectangular region with a constant length L and a variable height H. A linear relation between the driving force X and a height H

$$\rho X = d_1 + d_2 H \tag{77}$$

follows from Eq. (64), where $d_1 = c_1 + c_2 L$ and $d_2 = c_3 + c_4 L$ are coefficients. Below we consider the case when $d_1 > 0, d_2 < 0$. The other cases can be analyzed in a similar way. The thermodynamic fracture criterion (43) and the extremum principle (45) are as follows

$$y_1 = d_1 + d_2 H - \frac{\Gamma}{H} \geqslant 0, \tag{78}$$

$$y_2 = (d_1 + d_2 H - E_a) 2HL - \Gamma 2L; \ \rightarrow \ \max_H. \tag{79}$$

From a physical viewpoint we should add the following constraints:

$$y_2 = (d_1 + d_2 H - E_a) 2HL - \Gamma 2L < 0, \tag{80}$$

which defines a region where the kinetic equation is valid [see Eq. $(44)_2$], and

$$b \leqslant H \leqslant H_{\max} \tag{81}$$

which defines a minimum and maximum admissible values of H. From the condition $\frac{\partial y_2}{\partial H} = 0$ we have

$$H^{\diamond} = \frac{E_a - d_1}{2d_2}, \quad \frac{\partial^2 y_2(H^{\diamond})}{\partial^2 H} = 4d_2 L < 0. \tag{82}$$

Hence, at $H = H^{\diamond}$ the function y_2 has a maximum. If this $H^{\diamond} \geqslant 0$ and $H^{\diamond}$ is met for all the constraints (78), (80), (81), then $H^{\diamond}$ is the actual height. If $H^{\diamond}$ does not meet some of the constraints then the actual H must be found at the boundary of variation of H determined by the constraints. If $H^{\diamond} < 0$ then a maximum value of y_2 is reached at the smallest H which satisfies all the constraints. The thermodynamic criterion (78) restricts the admissible values of H between two roots H_1 and H_2 of equation $y_1 = 0$,

$$H_1 \leqslant H \leqslant H_2, \tag{83}$$

$$0 < H_1 = \frac{-d_1 + \sqrt{d_1^2 + 4\Gamma d_2}}{2d_2}, \quad 0 < H_2 = \frac{-d_1 - \sqrt{d_1^2 + 4\Gamma d_2}}{2d_2}, \tag{84}$$

as $d_1 > 0, d_2 < 0$. At $H^{\diamond} < 0$ inequality (80) is fulfilled for any H. Thus, the smallest $H = H_o$ which satisfies constraints (81) and (83) is $H_o = \max\{b, H_1\}$. At $H_1 > H_{\max}$ or $H_2 < b$ or $d_1^2 + 4\Gamma d_2 < 0$ a solution does not exist, i.e. fracture under a given external force is impossible.

Consequently, the following typical cases in the determination of two characteristic sizes of fracture region are found: from the principle of the minimum of transformation time and kinetic equation solely without any constraints; from the principle of the minimum of transforming mass and the thermodynamic fracture criterion; as an interatomic distance and from the thermodynamic criterion; as the size of a sample.

It is necessary to note that for geometrically similar samples the driving force φ is constant if the external stress, elastic moduli and yield stress are constant. For example, in order to satisfy the thermodynamic criterion (70) with the fracture region consisting of domains I, II ($X = 2.5$ MPa), the height of this region at $\Gamma = 1.2$ Pa·m (for our two-dimensional problem the size of a sample in the third direction is assumed to be equal to unit) should be

$$H \geqslant \frac{\Gamma}{X} = 0.48 \cdot 10^{-6}\text{m}. \tag{85}$$

6. Interaction between fracture and phase transitions

High stresses due to relatively large transformation strain may result in a fracture, namely crack and void nucleation and growth, see examples in Hornbogen (1991). On the other hand, a stress concentrator at the crack tip can induce PT (Stump and Budiansky, 1989; Bulbich, 1992). Due to PT one obtains higher toughness; this is the so-called transformation toughening phenomenon.

To illustrate some types of interaction between PT and fracture we solved several model problems under the same boundary conditions as above in Fig. 24; results are summarized in Table 2. For fracture in region II the mechanical driving force $\varphi = 3.38$ MPa. However, if fracture occurs in region II after PT in region I + II, then PT decreases the driving force for fracture up to the value 1.35 MPa. Fracture in region II + IV decreases the driving force for PT in region I up to −8.06 MPa (due to unloading in this region) and increases the driving force for PT in region V and especially VI.

As the last class of problems we consider competition between fracture and PT for time independent kinetics. We compare 4 different processes: PT region I + II or in I–IV, and fracture in region II or in region II + IV. Assume that each of these processes is thermodynamically admissible, i.e. the thermodynamic criterion of SC is fulfilled at chosen values of the surface energy and the dissipative threshold. We have to select which process will occur in reality. We assume that the best solution is the stable one. According to extremum principle (42) for the determination of the stable deformation process, for the prescribed fixed stresses the larger the displacement averaged over line BC the more stable is the process. Consequently, fracture in region II + IV will occur as the most stable process (Table 3). If for such a process the thermodynamic fracture criterion is not satisfied, then PT in region I–IV will

Table 2
Driving force φ for various scenarios of fracture and PT

The first process	φ, MPa	The second process	φ, MPa	
PT in I, II	7.01	Fracture in II	1.35	
—		Fracture in II	3.38	
Fracture in II, IV	6.48	PT in I	−8.06	
Fracture in II, IV	6.48	PT in V	10.17	
Fracture in II, IV	6.48	PT in VI	12.62	

Table 3
Normal displacement, averaged over BC, for various processes

The process	Displacement u_{BC}	φ, MPa	
PT in I, II	$0.7491\ 10^{-3}$	7.01	
PT in I, II, III, IV	$0.988\ 10^{-3}$	8.81	
Fracture in II	$0.9659\ 10^{-3}$	3.38	
Fracture in II, IV	$2.415\ 10^{-3}$	6.48	

 PT;  fracture.

occur. If PT in region I + II and fracture in region II are only thermodynamically possible, then fracture will occur. Consequently, in addition to the thermodynamic fracture criterion one needs the global fracture criterion based on stability analysis, similar to PT.

7. Concluding remarks

In the paper, a unified numerical approach to such, from a physical point of view different, SC as temperature-, stress- and strain-induced PT, deformation twinning and fracture in elastoplastic materials is developed. Both small and finite strain formulations are included in a similar way. The approach suggested is based on the solution of elastoplastic and thermal boundary-value problems when we vary transformation deformation gradient and/or elastic properties from initial to final values in a transforming region. The driving force for SC is calculated using stress, strain and temperature fields obtained and is applied to the estimation of the thermodynamical possibility of SC, determination of an actual PT region (solutions for various possible transforming regions have to be obtained) and time of SC. Both time independent and time dependent kinetics are considered. For time independent kinetics, to overcome the nonuniqueness of solution of boundary-value problems due to competition between PT and plasticity and/or fracture, the global PT and fracture criteria based on stability analysis are applied. Possible sliding or decohesion at the interface is taken into account by considering contact problems.

The applicability of the approach developed is illustrated by a solution of a number of two-dimensional model elastoplastic boundary-value problems, in particular, layer by layer PT progress in a cylindrical specimen, adiabatic strain-induced PT at the shear-band intersection and in a spherical particle embedded in a cylindrical specimen, appearance and growth of temperature-induced martensitic plate in an austenitic matrix, appearance of a single twin in a space under applied shear stress or displacement, fracture in a sample with an edge notch and an interaction between PT and fracture in the same sample. Despite the fact that most of the real problems are three-dimensional, consideration of the above two-dimensional problems allows us to understand the importance of various factors, in particular, a very complex and nontrivial field variation and its effect on the driving force for SC, peculiarity of the interaction between PT, twinning, fracture and plasticity, effect of strain hardening and adiabatic heating, formation of a discrete microstructure at PT and fracture (in particular, void nucleation ahead of the crack tip rather than continuous crack propagation). Some of the numerical results for the driving force are approximated analytically and applied to the analytical determination of the geometry of PT and fracture zones based on the corresponding extremum principle.

The same approach can be applied to the solution of three-dimensional problems, however it is much more time consuming. The possibility of formation of several martensitic variants in the transforming region and the real crystallography of martensitic PT have to be taken into account. The uniqueness and mesh dependence of the solutions have to be studied as well.

Complete modeling of the formation of a microstructure requires solution of the problem of topological optimization. Another approach based on a generalization of the Landau-Ginzburg theory for plastic materials (which has to be developed) will probably be more convenient.

Acknowledgements

V.I.L. and A.V.I. gratefully acknowledge the support of the German Research Society (DFG) and Volkswagen Foundation, grant I/70283. V.I.L. also acknowledge the support of Texas Tech University. Critical comments of Professor F.D. Fischer (Montanuniversität Leoben, Austria) are very much appreciated.

References

Atluri, S.N., 1997. Structural Integrity & Durability. Tech Science Press, Forsyth.

Bažant, Z.P., 1989. Stable states and stable paths of propagating of damage zones and interactive fractures. In: Mazars, J., Bažant, Z.P. (Eds.), Cracking and Damage. Elsevier, London, pp. 183–206.

Bulbich, A.A., 1992. Nucleation on the crack tip and transformation toughness in crystals undergoing structural phase transitions. Journal of Materials Science 27, 1070.

Cuitino, A., Ortiz, M., 1992. A material-independent method for extending stress update algorithms from small-strain plasticity to finite with multiplicative kinematics. Eng. Comput. 9, 437.

Dafalias, Y.F., 1984. The plastic spin concept and a simple illustration of its role in finite plastic transformations. Mechanics of Materials 3, 223.

Ganghoffer, J.F., Denis, S., Gautier, E., Simon, A., Simonsson, K., Sjöström, S., 1991. Micromechanical simulation of a martensitic transformation by finite element. Journal de Physique IV, Colloque C4 1, 83–88.

Haezebrouck, D.M., 1987. Nucleation and growth of a single martensitic particle. Northwestern University, Materials Research Center, Steel Research Group, Evanston.

Hornbogen, E., 1991. Legierungen mit Formgedächtnis. Rheinisch-Westfälische Akademie der Wissenschaften (Vorträge, 338), Westdeutcher Verlag.

Idesman, A.V., Levitas, V.I., 1995. Finite element procedure for solving contact thermoplastic problems at large strain, normal and high pressures. Comp. Meth. Appl. Mech. Eng. 126, 39.

Idesman, A.V., Levitas, V.I., Stein, E., 1997a. Simulation of martensitic phase transition progress with continuous and discontinuous displacements at the interface. Computational Materials Science 9, 64.

Idesman, A.V., Levitas, V.I., Stein, E., 1997b. Finite element simulation of martensitic phase transition in elastoplastic material at finite strains. In: Onate, E. et al. (Eds.), Proceedings of 5th International Conference on Num. Meth. in Plasticity (COMPLAS 5), Barcelona. Pineridge Press, Swansea, pp. 1323–1328.

Idesman, A.V., Levitas, V.I., Stein, E., 1999a. Computational methods for elastoplastic materials with martensitic phase transitions. In: Bruhns, O.T., Stein, E. (Eds.), Proceedings of the IUTAM Symposium on Micro- and Macrostructural Aspects of Thermoplasticity, Bochum, Germany, 25–29 August 1997. Kluwer Academic Publisher, Dordrecht, Netherlands, pp. 373–382.

Idesman, A.V., Levitas, V.I., Stein, E., 1999b. Elastoplastic materials with martensitic phase transition and twinning at finite strains: numerical solution with the finite element method. Comp. Meth. Appl. Mech. Eng. 173 (1–2), 71.

Leblond, J.B., Devaux, J., Devaux, J.C., 1989. Mathematical modeling of transformation plasticity in steels I: Case of ideal-plastic phases, Int. J. Plasticity 5, 551.

Leblond, J.B., 1989. Mathematical modeling of transformation plasticity in steels II: coupling with strain hardening phenomena, Int. J. Plasticity 5, 573.

Levitas, V.I., 1995. The postulate of realizability: formulation and applications to post-bifurcation behavior and phase transitions in elastoplastic materials. Parts I and II. Int. J. Eng. Sci. 33, 921.
Levitas, V.I., 1996. Large Deformation of Materials with Complex Rheological Properties at Normal and High Pressure. Nova Science Publishers, New York.
Levitas, V.I., 1997. Phase transitions in elastoplastic materials: continuum thermomechanical theory and examples of control. Parts I and II. J. Mech. Phys. Solids Part I: 45(6), 923; Part II: 45(7), 1203.
Levitas, V.I., 1998a. Thermomechanical theory of martensitic phase transformations in inelastic materials. Int. J. Solids Struct. 35 (9–10), 889.
Levitas, V.I., 1998b. Thermomechanics and kinetics of generalized second-order phase transitions in inelastic materials. Application to ductile fracture. Mech. Res. Commun. 25 (4), 427–436.
Levitas, V.I., 1998c. General thermomechanical and kinetic approach to structural changes in inelastic material. In: Khan, A. (Ed.), Constitutive and Damage Modeling of Inelastic Deformation and Phase Transformation, Proceedings of "Plasticity'99". Neat Press Fulton, Maryland, pp. 235–238.
Levitas, V.I., 1998d. A new look at the problem of plastic spin based on stability analysis. J. Mech. Phys. Solids 46 (3), 557–590.
Levitas, V.I., 2000a. Structural changes without stable intermediate state in inelastic material. Part I. General thermomechanical and kinetic approaches. Int. J. Plasticity 16, 805–849.
Levitas, V.I., 2000b. Structural changes without stable intermediate state in inelastic material. Part II. Applications to displacive and diffusional-displacive phase transformations, strain-induced chemical reactions and ductile fracture. Int. J. Plasticity 16, 851–892.
Levitas V.I. & Idesman A.V., 1998. Ductile fracture: new thermomechanical and kinetic approach and numerical study. In: Mahnken, R. (Eds.), Theoretische und Numerische Methoden in der Angewandten Mechanik mit Praxisbeispielen. Festschrift anlässlich der Emeritierung von Prof. Erwin Stein. Universität Hannover. Institut für Baumechanik und Numerische Mechanik, IBNM-Bericht 98/4, Hannover, pp. 65–72.
Levitas, V.I., Idesman, A.V., Stein, E., 1998a. Finite element simulation of martensitic phase transitions in elastoplastic materials. Int. J. Solids Struct. 35 (9–10), 855.
Levitas, V.I., Nesterenko, V.F., Meyers, M.A., 1998b. Strain-induced structural changes and chemical reactions. Parts I and II. Acta Materialia 46 (16), 5929.
Levitas, V.I., Idesman, A.V., Olson, G.B., 1999. Continuum modeling of strain-induced martensitic transformation at shear-band intersections. Acta Materialia 47 (1), 219.
Levitas V. I., Idesman A. V., Olson G. B., Stein E., 2000. FEM modeling of stress-strain fields, thermodynamics and kinetics of martensitic plate growth in elastoplastic material. Acta Metall. Mater. (submitted).
Marketz, F., Fischer, F.D., 1994a. A micromechanical study on the coupling effect between microplastic deformation and martensitic transformation. Comput. Mater. Science 3, 307.
Marketz, F., Fischer, F.D., 1994b. Micromechanical modelling of stress-assisted martensitic transformation. Modelling Simul. Mater. Sci. Eng. 2, 1017.
Nishiyama, Z., 1978. Martensitic Transformation. Academic Press, New York.
Olson, G.B., Cohen, M., 1972. A mechanism for the strain-induced nucleation of martensitic transformation. J. Less-Common Metals 28, 107.
Olson, G.B., 1984. Transformation plasticity and the stability of plastic flow. In: Krauss, G. (Ed.), Deformation, Processing and Structure. ASM International, Warrendale, PA, pp. 391–424.
Olson, G.B., Cohen, M., 1986. Dislocation theory of martensitic transformations. In: Nabarro, F.R.N. (Ed.), Dislocations in solids, vol. 7. Chap, North-Holland, Amsterdam, pp. 295–.
Reisner, G., Werner, E.A., Fischer, F.D., 1998. Micromechanical modelling of martensitic transformation in random microstructures. Int. J. Solids and Structures 35, 2457.
Schlögl, S.M., Fischer, F.D., 1997. The role of slip and twinning on the deformation behaviour of polysynthetically twinned (PST) crystals of TiAl — a micromechanical model. Philosophical Magazine A 75, 621.
Staroselsky, A., Anand, L., 1998. Inelastic deformation of polycrystalline face centered cubic materials by slip and twinning. J. Mech. Phys. Solids 46, 671.
Stringfellow, R.G., Parks, D.M., Olson, G.B., 1992. A constitutive model for transformation plasticity accompanying strain-induced martensitic transformations in metastable austenitic steels. Acta Metall. Mater. 40, 1703.

Stump, D.M., Budiansky, B., 1989. Crack-growth resistance in transformation-toughened ceramics. Int. J. Solids Structures 25 (6), 635.
Weber, G., Anand, L., 1990. Finite deformation constitutive equations and a time integration procedure for isotropic hyperelastic-viscoplastic solids. Comput. Methods Appl. Mech. Engrg. 79, 173–202.
Wechsler, M.S., Lieberman, D.S., Read, T.A., 1953. On the theory on the formation of martensite. J. Metals, Trans. AIME 197, 1503.